Bioactive Materials 19 (2023) 88–102

Contents lists available at ScienceDirect

Bioactive Materials

journal homepage: www.keaipublishing.com/en/journals/bioactive-materials

Seamless and early gap healing of osteochondral defects by autologous mosaicplasty combined with bioactive supramolecular nanofiber-enabled gelatin methacryloyl (BSN-GelMA) hydrogel

Hongwei Wu [a,b,c,1], Yuna Shang [e,1], Wei Sun [a,c,1], Xinyi Ouyang [f], Wenyan Zhou [a,c], Jieji Lu [c], Shuhui Yang [c], Wei Wei [g], Xudong Yao [g], Xiaozhao Wang [a,c], Xianzhu Zhang [a,c], Yishan Chen [a,c], Qiulin He [a,c], Zhimou Yang [h,**], Hongwei Ouyang [a,b,c,d,*]

[a] Dr. Li Dak Sum & Yip Yio Chin Center for Stem Cells and Regenerative Medicine, and Department of Orthopedic Surgery of the Second Affiliated Hospital, Zhejiang University School of Medicine, Hangzhou, China
[b] Department of Sports Medicine, Zhejiang University School of Medicine, Hangzhou, China
[c] Zhejiang University-University of Edinburgh Institute, Zhejiang University School of Medicine, and Key Laboratory of Tissue Engineering and Regenerative Medicine of Zhejiang Province, Zhejiang University School of Medicine, Hangzhou, China
[d] China Orthopedic Regenerative Medicine Group (CORMed), Hangzhou, China
[e] College of Chemistry, Tianjin Normal University, Tianjin, 300387, PR China
[f] Faculty of Science, The University of Melbourne, Parkville, VIC, 3010, Australia
[g] International Institutes of Medicine, The 4th Affiliated Hospital of Zhejiang University School of Medicine, Yiwu, Zhejiang, China
[h] Key Laboratory of Bioactive Materials, Ministry of Education, State Key Laboratory of Medicinal Chemical Biology, College of Life Sciences, Collaborative Innovation Center of Chemical Science and Engineering, and National Institute of Functional Materials, Nankai University, Tianjin, 300071, China

ARTICLE INFO

Keywords:
Mosaicplasty
Osteochondral integration
Bioactive supramolecular nanofiber
GelMA hydrogel
Tissue engineering

ABSTRACT

Autologous mosaicplasty is a common approach used to treat osteochondral defects in clinical practice. Gap integration between host and transplanted plugs requires bone tissue reservation and hyaline cartilage regeneration without uneven surface, graft necrosis and sclerosis. However, poor gap integration is a serious concern, which eventually leads to deterioration of joint function. To deal with such complications, this study has developed a strategy to effectively enhance integration of the gap region following mosaicplasty by applying injectable bioactive supramolecular nanofiber-enabled gelatin methacryloyl (GelMA) hydrogel (BSN-GelMA). A rabbit osteochondral defect model demonstrated that BSN-GelMA achieved seamless osteochondral healing in the gap region between plugs of osteochondral defects following mosaicplasty, as early as six weeks. Moreover, the International Cartilage Repair Society score, histology score, glycosaminoglycan content, subchondral bone volume, and collagen II expression were observed to be the highest in the gap region of BSN-GelMA treated group. This improved outcome was due to bio-interactive materials, which acted as tissue fillers to bridge the gap, prevent cartilage degeneration, and promote graft survival and migration of bone marrow mesenchymal stem cells by releasing bioactive supramolecular nanofibers from the GelMA hydrogel. This study provides a powerful and applicable approach to improve gap integration after autologous mosaicplasty. It is also a promising off-the-shelf bioactive material for cell-free in situ tissue regeneration.

Abbreviations: BSN-GelMA, bioactive supramolecular nanofiber-enabled gelatin methacryloyl (BSN-GelMA); AOT, autograft osteochondral transplantation; IGF-1, Insulin-like growth factor-1; rBMSCs, rabbit bone marrow mesenchymal stem cells; GAG, glycosaminoglycan.

Peer review under responsibility of KeAi Communications Co., Ltd.

* Corresponding author. Dr. Li Dak Sum & Yip Yio Chin Center for Stem Cells and Regenerative Medicine, and Key Laboratory of Tissue Engineering and Regenerative Medicine of Zhejiang Province, Zhejiang University School of Medicine, Hangzhou 320000, China.
** Corresponding author.
E-mail addresses: yangzm@nankai.edu.cn (Z. Yang), hwoy@zju.edu.cn (H. Ouyang).
[1] These authors contributed equally to this work.

https://doi.org/10.1016/j.bioactmat.2022.03.038
Received 29 December 2021; Received in revised form 4 March 2022; Accepted 25 March 2022
Available online 5 April 2022

1. Introduction

Autograft osteochondral transfer (AOT) mosaicplasty, one of the most extensively applied surgical techniques in clinical practice, involves transplantation of multiple small cylindrical autologous osteochondral units as plugs from less load-bearing sites to the defect sites [1–3]. The operation offers several advantages over other repair techniques such as primary repair, less incision and injury, lower cost, and quick recovery [4–7]. However, integration of gaps between plugs of osteochondral defects remains a challenge. Inappropriate integration of a gap in osteochondral defects ultimately leads to the formation of fibrotic tissues, especially fibrocartilage [8,9]. Besides, an absence of a filling in the gap, degeneration of the grafted tissues, and a potential dead space between grafts may further prevent gap integration and limit the quality of repair [10–14]. Gap integration of AOT relies on autologous cell migration from adjacent tissues, maximum volume retention of extracellular matrix, and survival of graft *in vivo* [15–17]. Poor graft survival usually results in necrosis, apoptosis, or osteosclerosis, which eventually deteriorate the joint function and treatment outcome [14,18]. It was reported that approximately one-third of the joint bone after mosaicplasty surface was nonviable, followed by 24% rate of marginal zone cell death, and 9% rate of interposed dead space between grafts [10]. Besides, it may be difficult to fuse together adjacent cartilages because of the proteoglycan nature of the main components of the cartilage matrix [11,13,19]. Therefore, it is important to search for further remedies to resolve the problem of gap integration.

Previous studies have mainly focused on improving surgical techniques [4,9,20–25]; however, only a few studies have attempted to improve the gap integration of grafts following mosaicplasty using a tissue engineering approach. In the tissue engineering field, natural growth factor-loaded hydrogel scaffolds have been proved to improve cell viability and osteochondral regeneration [26–30]. However, because they are easily inactivated, it is difficult to maintain their biological activity when combined with scaffold materials, which greatly hinder their long-term effects *in vivo* [31–34]. Furthermore, the biological effects of many growth factors are concentration dependent. Hence, maintaining an appropriate concentration *in vivo* is crucial [35]. Therefore, it is necessary to develop alternative bioactive materials to replace traditional scaffold materials loaded with natural growth factors. Recently, bioactive supramolecular nanofibers have shown a great potential in tissue engineering and regenerative medicine, and are the best alternatives to natural growth factors [36–38]. Supramolecular nanofibers formed by non-covalent interactions have excellent tissue retention and improved bioavailability [39]. Compared to natural growth factors, they are less prone to be inactivated by endogenous digestion enzymes and are more cost-effective [40]. Recently, Stupp and colleagues have shown that synthesized amphiphile bioactive supramolecular nanofibers, which could activate the transmembrane receptor (β1-integrin) and the basic fibroblast growth factor 2 receptor, was able to promote functional recovery in a mouse spinal cord injury model by enhancing vascular growth, axonal regeneration, etc. [41]. This epochal study demonstrated that bioactive supramolecular nanofibers have a great potential for therapeutic applications.

Insulin-like growth factor-1(IGF-1), a hormone with anti-apoptotic and anti-inflammatory properties, can promote cell metabolism and growth [42]. Besides, IGF-1 was shown to promote extracellular matrix generation of chondrocytes and stimulate proliferation and chondrogenic differentiation of bone marrow mesenchymal stem cells (BMSCs) via paracrine mechanisms, thus improve osteochondral healing [29,43]. Previous studies revealed that the delivery of IGF-1 could retain adjacent glycosaminoglycan (GAG) and cell content in a rabbit osteochondral defect model [30,44], suggesting that IGF-1 may play an important role in balancing proteoglycan synthesis and breakdown, as well as regulating the homeostasis of native cartilage tissue. A recent study has indicated that IGF-1 could improve the integration of cartilage grafts with native cartilage by enhancing the migration of chondrocytes across the graft-host interface [45], suggesting that IGF-1 possesses the capacity to promote cell migration. These findings demonstrate that IGF-1 has the potential to enhance the activity of BMSCs and also plays a role in osteogenic/chondrogenic differentiation of BMSCs to improve osteochondral healing and gap space integration after AOT mosaicplasty.

Based on the above-mentioned findings, we developed a novel strategy to heal the gaps between osteochondral plugs promptly and seamlessly after mosaicplasty. This strategy utilizes an injectable photocuring GelMA hydrogel loaded with bioactive supramolecular nanofibers that mimic IGF-1 [40]. IGF-1 bioactive supramolecular nanofibers (IGF-1bsn) can bind to IGF-1 receptors and their bioavailability is greatly improved due to their high stability and tissue retention, laying a solid foundation towards improving their biological activities *in vivo*. In this study, we demonstrated that IGF-1bsn could enhance rabbit BMSC migration *in vitro*. IGF-1bsn–incorporated GelMA hydrogel accomplished seamless osteochondral integration after mosaicplasty as early as six weeks in a rabbit knee joint osteochondral defect model. This approach provides a powerful strategy and cost-effective off-the-shelf product for the treatment of osteochondral integration after mosaicplasty.

2. Experimental section

2.1. Materials

Primary rabbit BMSCs (rBMSCs) were harvested from femur bone marrow of 3 weeks old rabbit. Cell culture medium (CM) and fetal bovine serum were purchased from Gibico (USA). Cells at passage 3–5 were used in the following experiments. Recombinant IGF-1 protein was purchased from Peprotech (100–11, Peprotech, USA). Cell Counting Kit 8 (CCK-8) was purchased from Dojindo (Shanghai, China). Live/dead reagent, Phalloidine and Second antibody Alexa Flour 555 were purchased from Thermofisher. Annexin V-FITC apoptosis assay kit was purchased from Absin (Shanghai, China). Type II collagen antibody was purchased from Norvas (NB600-844, USA).

2.2. Synthesis of IGF-1 bioactive supramolecular nanofiber

The IGF-1 bioactive supramolecular nanofiber was synthesized as previously described [40]. Briefly, 2-chlorotriacyl chloride resin and amino acids whose N-terminal is protected by Fmoc, and the side chain is properly protected. All peptide derivatives were synthesized by the standard solid phase peptide synthesis (SPPS). Compounds were uniformly dispersed in endotoxin-free PBS, and 2 equiv of sodium carbonate was added to adjust the pH to 7.4 to form a suspension with a concentration of 0.5 wt %. Hydrogel formation was observed after the suspension was heated and cooled for 5 min.

2.3. Transmission electron microscopy

Firstly, 10 μL (1 mmol/L) of hydrogel was placed on the carbon-coated copper grids with a pipette. The gel was washed twice with water and dried with a filter paper. We stained the thin layer of hydrogel with uranium acetate for 1 min. In the end, the samples were transferred to a desiccator to dry overnight.

2.4. Fourier transform infrared (FTIR) spectroscopy

The gels were deposited on potassium bromide tablets and dried at ambient conditions. The non-covalent interactions and conformations of samples were detected by FTIR spectroscopy (TENSOR-27, Bruker) at room temperature.

2.5. Preparation of GelMA hydrogel and GelMA/IGF-1bsn hydrogel

GelMA was synthesized according to previously illustrated protocols [46]. A photo-initiator LAP (lithium phenyl-2,4,6-trimethylbenzoylphosphinate) was added to GelMA before use at a final concentration of 8.5 mM. GelMA/IGF-1bsn hydrogel was prepared by heating the stock IGF-1bsn suspension (1 mmol/L) until transparent and then diluted into GelMA solution to a final concentration of 10 μmol/L. Various concentration of IGF-1bsn in following experiments was further diluted from this stock solution.

2.6. Cell viability assay

To verify the biocompatibility of IGF-1bsn and IGF-1bsn contained hydrogel, rBMSC suspension was added on the surface of 10% GelMA hydrogel supplemented with different doses of IGF-1bsn (0, 10, 50, 100, 200, 400 nM, 3 wells each group) in 24-well plates (1×10^4 cells/well). rBMSCs cultured on tissue culture plate were used as control. 72 h after the cultivation, the viability of rBMSCs was evaluated by live/dead staining using Calcein AM (fluorescent green for live cells) and PI dyes (fluorescent red for dead cells) for 20-min incubation at 37°C. Images were taken by inverted fluorescence microscope (Leica, German).

2.7. Cell proliferation assay

To investigate the effect of IGF-1bsn on the proliferation of rBMSCs *in vitro*, a Cell Counting Kit 8 (CCK-8) assay and a colony forming unit (CFU) assay were performed. rBMSCs were seeded in 96-well plates (2.5×10^3 cells/well) and cultured in low glucose culture medium. Then, the cells were treated with different doses of IGF-1bsn (0, 10, 50, 100, 200 nM, 5 wells each group) for 1, 3, 5 days. To compare the cell amount, rBMSCs in each well were incubated with 10 μL CCK-8 solution (Dojindo, shanghai, China) diluted in CM in the incubator for 4 h. Then, the optical density (OD) values at 450 nm were read with a microplate reader (Tecan's Spark, Australia). Cells for CFU test were cultured for 10 days, then rBMSCs were stained with 0.5% (v/v) crystal violet solution at room temperature for 10 min. Images were taken by stereoscope and inverted fluorescence microscope (Leica, German) where the size of colonies with a diameter over 1 mm could be calculated by ImageJ.

2.8. Cell migration assay

To study the effect of IGF-1bsn on migration of rBMSCs, the 2D cell scratch assay and 3D cell migration assay was performed. rBMSCs were seeded in 6-well plates (2×10^5 cells/well) and cultured with CM containing different concentration of IGF-1bsn (0, 10, 50, 100, 200 nM) for 12 h. The cells which migrated to the scratches were imaged and counted at 0, 12 h under inverted fluorescence microscope. For 3D cell migration assay, the rBMSC suspension were resuspended with GelMA hydrogel at a final concentration of 1×10^6 cells/ml. The cell-hydrogel suspension was then crosslinked by UV light in an 8-well chamber slide. The 3D cell-hydrogel constructs were cultured in low glucose culture medium with or without 100 nM IGF-1bsn. The constructs were collected and stained with phalloidine on 1, 3 and 5 days, respectively. Then the constructs were imaged and three dimensions reconstructed under confocal microscopy (Zeiss 880, German). The cell migration distance from bottom to 500 μm above in the IGF-1bsn group was calculated and compared with each other.

2.9. Cell apoptosis assay

To investigate the anti-apoptosis effect of IGF-1bsn on rBMSCs *in vitro*, a cell apoptosis assay was performed. rBMSCs were seeded in 6-well plates (1×10^5 cells/well) and cultured with CM. Then the cells were treated with media containing 200 μM H_2O_2 and 1% P/S for 4 h to realize oxidative damage. Then they were rinsed by PBS and cultured with CM containing different doses of IGF-1bsn (0, 50, 100, 200, 400 nM, 3 wells each group) for 24 h. After that, the cells were collected and Annexin V-FITC apoptosis assay kit (Absin, Shanghai, China) was used to detect the apoptosis rate by following the protocol. After IGF-1bsn treatment, apoptosis related gene expression of Bcl-2, Bax, Bad mRNA in rBMSCs was determined by quantitative real-time polymerase chain reaction (qRT-PCR) with total RNA extracted from cells and the primers listed in Table S1.

2.10. In vivo mosaicplasty of osteochondral defects in rabbits

In this project, 18 News Zealand rabbits (male, 3 Kg in average) were collected from animal center in Zhejiang University, Zijingang Campus. They were treated under standard animal ethic guidelines approved by the Zhejiang University Ethics Committee (ZJU20210248). Rabbits were anesthetized with intravenous pentobarbital (20 mg/kg) and Zoletil (10 mg/kg). Medial parapatellar approach was operated on the knee joints with a trephine to create a cylinder-shape osteochondral defect with 3.5 mm in diameter and 3 mm deep at the trochlear groove, referring to previous study [47,48]. After that, the autologous osteochondral graft with the diameter of 2.5 mm was reimplanted in situ, leaving a gap of 0.5 mm wide between the host bone and the graft. The gap was left without any treatment in the blank group, while the gap of other groups was filled with GelMA hydrogel (GelMA group) or GelMA/IGF-1bsn (10 μM/ml) hydrogel (BSN-GelMA group). Then the wound was closed and the rabbits were sent back to cages for recovering. At 6 and 12 weeks, half of the rabbits were sacrificed with excessive intravenous pentobarbital. Samples were harvested for subsequent examination (n = 6 each group).

2.11. ICRS scoring system for macroscopic evaluation

International Cartilage Repair Society (ICRS) scoring system was applied to examine outcome of the samples according to a previously established scoring standard (Table S2) [49]. Three independent graders were asked for scoring who were not involved in the study and were blind to the groups (n = 6 per group). Images from macroscopic, and H&E staining were observed and scored by graders.

2.12. Micro-computed tomography analysis

The knee joints were fixed in 4% paraformaldehyde for 2 days (pH = 7.0, room temperature) after harvest. Samples (n = 6 per group) were scanned by small animal *in vivo* Micro Computed Tomography (Netherland, Milabs) and subsequently reconstructed. A constant region of interest with defect site 3.5 mm in diameter and 3 mm deep was assigned. The reconstructed profiles were visualized and analyzed afterwards. For each group, a representative sample was randomly chosen. For gap defect calculation, 4 samples in each group were randomly selected. The area of bone defects displaying in the coronal section on both sides were measured by Image J. The original gap was 3 mm in depth and 0.5 mm in width. Then the percentage of gap defect was then calculated.

2.13. Histological staining and analysis

The samples in each group (n = 4 per group) were processed for histological staining and analysis. After being decalcified and embedded in paraffin, the samples were sliced to produce 7 μm histological sections. Following staining were performed for each sample: H&E staining for morphology; safranin-O and fast green (SF) staining for distinguishment of cartilage and bone tissues, as well as content of proteoglycan in cartilage; Masson's staining for collagen content. All slices were digitally photographed under High-Content Imaging System IXM-C after staining. Three authors performed the histology scores according to the previously reported standard criteria [50]. To detect the hyaline

cartilage in the graft after the transplantation, immunofluorescence staining for collagen II (1:200, Novus, NB600-844) was performed. After incubated with secondary antibodies (Alexa Flour 555, Thermofisher) and DAPI, the sections were then viewed under Zeiss LSM 880 Confocal Microscope system and the relative intensity of collagen II expression was calculated in each group.

2.14. Statistical analysis

Quantitative results from scorings and image analysis software are presented as mean ± standard deviations (SD). GraphPad Prism 8.0 software was applied to perform t-tests or one-way ANOVA analysis of variance tests. Statistically significant differences were shown as ns: non-significant, *p < 0.05, **p < 0.01, ***p < 0.001 and ****p < 0.0001.

3. Results

3.1. Molecular structure of IGF-1bsn

Previous studies have shown that the C-domain consisting of a dodecapeptide (GYGSSSRRAPQT) is a key binding site of IGF-1 receptor (IGF-1R) and plays an important role in regulating IGF-1 activity [51]. Therefore, we generated these dodecapeptides and covalently linked them to an assembly peptide, Nap-FFG, and obtained IGF-1 mimicking peptides, also known as IGF-1 bioactive supramolecular nanofibers (IGF-1bsn, Nap-FFGGYGSSSRRAPQT), which had a potential to self-assemble (Fig. 1A and B). IGF-1bsn could self-assemble into an opaque hydrogel by the heating-cooling process in PBS buffer (pH 7.4) at a concentration of 1 mmol/L (Fig. 1C). Transmission electron microscopy (TEM) images revealed that the microstructure was a three-dimensional network composed of nanofibers with a diameter of approximately 20 nm (Fig. 1D). Fourier transform infrared spectroscopy (FTIR) further showed the characteristic peaks of an amide I band at 1638 cm^{-1} and an amide III absorption band at approximately 1232 cm^{-1} (Fig. 1E), which corresponded to hydrogen-bonded β-sheet secondary structures of IGF-1bsn [52–54]. Fig. S1 showed the *in vitro* stability of the fibers. Results showed that the IGF-1 bioactive supramolecular nanofibers (IGF-1bsn) exhibited weak frequency dependence at the range of 0.1–100 rad s^{-1}, indicating good elasticity. The storage modulus (G′) was approximately an order of magnitude higher than their loss modulus (G″), which indicated the stable existence of nanofibers. In conclusion, IGF-1bsn has good stability under physiological condition. In vitro degradation of the nanofibers also showed that the IGF-1bsn remained above 26% after 24 h *in vitro* (Fig. S2).

3.2. Biological activity of IGF-1bsn in rabbit BMSCs

Our previous studies have shown that IGF-1bsn has a biological activity that was superior than that of IGF-1 in protecting human umbilical vein endothelial cells (HUVECs) from apoptosis [40]. Similar experiments were performed on rabbit BMSCs. The results of live/dead staining for cell viability demonstrated that the apoptosis rate was 84.97 ± 1.29 in control group, whereas it was only 4.73 ± 0.40 and 1.53 ± 0.45 in IGF-1 group and IGF-1bsn group, respectively (P < 0.001, Figs. S3A and S3B). To prove the biocompatibility of IGF-1bsn, we cultured rabbit BMSCs in a culture medium containing IGF-1bsn as well as on a GelMA hydrogel containing IGF-1bsn (Fig. S3C). Live/dead staining demonstrated that cell viability both in the 2D culture medium and on hydrogel was comparable at concentrations from 0 to 200 nM of IGF-1 bsn (Figs. S3D–S3E).

To verify the biological effects of IGF-1bsn on rabbit BMSCs, we performed CCK-8 cell experiments using different concentrations of IGF-1bsn (0, 10, 50, 100, and 200 nM) to observe its effect on cell proliferation. To exclude the influence of fetal bovine serum (FBS), three different concentrations of FBS were tested. The OD values were proportional to the total rBMSC numbers. Generally, there was no difference or only a mild increase observed in the IGF-1bsn–supplemented groups than in the control group during the first three days. On day 5, there was a significant increase in the 100 nM- and 200 nM-treated groups (Fig. S4A). These data revealed that IGF-1bsn promoted BMSC proliferation in a mild and slow manner, even at low FBS concentrations (Figs. S4B and S4C).

The proliferation ability of the rBMSCs was also investigated using a

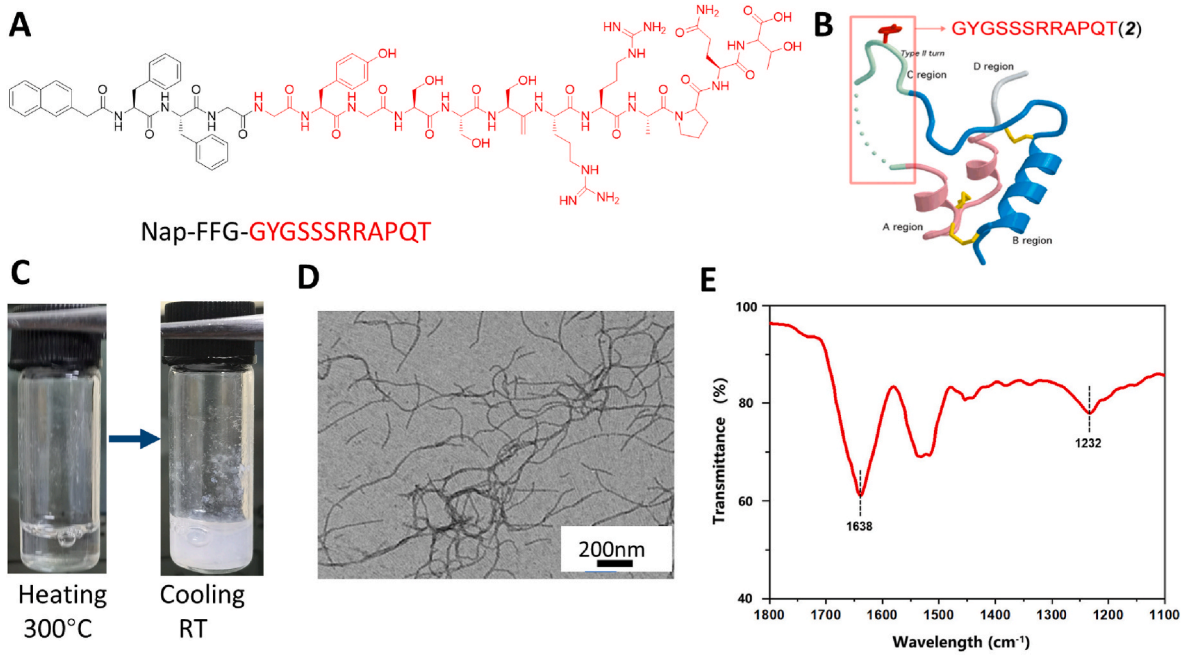

Fig. 1. Characterization of bioactive supramolecular nanofibers (bsn). (A) Chemical structure of bsn. (B) Ribbon structure of human IGF-1 protein. The C-region of the protein is shown in light green and is denoted by the box. (C) Optical images showing the transparent suspension of bsn after heating turning opaque after cooling at room temperature. (D) TEM image of the bsn suspension. Scale bar = 200 nm. (E) FTIR spectrum of bsn.

cloning forming unit (CFU) assay. Fig. S5 shows representative images from each group after 10 days of cell culture. The number of clone-forming units was the highest in the 100 nM-treated group. Percentage of the clone forming area of the cells in the 100 nM treatment group was the highest among all the groups ((Fig. S5B). After staining with crystal violet solution, the OD value in the 100 nM treatment group (0.1489 ± 0.0117) was significantly higher than that in the 0 nM group (0.1274 ± 0.0060) ((Fig. S5C). These results were consistent with the CCK-8 results, indicating that 100 nM of IGF-1bsn might be an optimal concentration for examining cell proliferation *in vitro*.

3.3. IGF-1bsn enhances the migration of BMSCs in vitro

To assess the migration ability of BMSCs under stimulation with different doses of IGF-1bsn, a scratch assay was performed using 2D culture and fluorescence staining was carried out employing 3D hydrogel culture. On the 2D tissue culture plate with 1% FBS in culture medium, the results indicated that the migrated cells in 50, 100, and 200 nM IGF-1bsn groups (54 ± 1.57, 64.33 ± 2.14, 63.67 ± 2.73, respectively) were significantly higher than those in the control group (48 ± 3.75) (Fig. 2A and B). Even in culture conditions with 0% FBS, the number of migrated cells in the 50–400 nM group was significantly higher than that in the control group. The number of migrated cells in the 200 nM group was the highest among all the groups ($P < 0.0001$) (Supplementary Fig. 6B).

Therefore, we used a culture medium containing 200 nM of IGF-1bsn to observe cell migration in the hydrogel; the regular medium was set as a control (Fig. 2C and D). Fluorescence staining images showed that there was a significant difference between the IGF-1bsn–treated group and control group in terms of average distance of cell migration on day 3 and day 5. The distance achieved in IGF-1bsn group on day 3 and day 5 was 240.0 ± 5.0 μm and 253.3 ± 7.6 μm, respectively, whereas it was

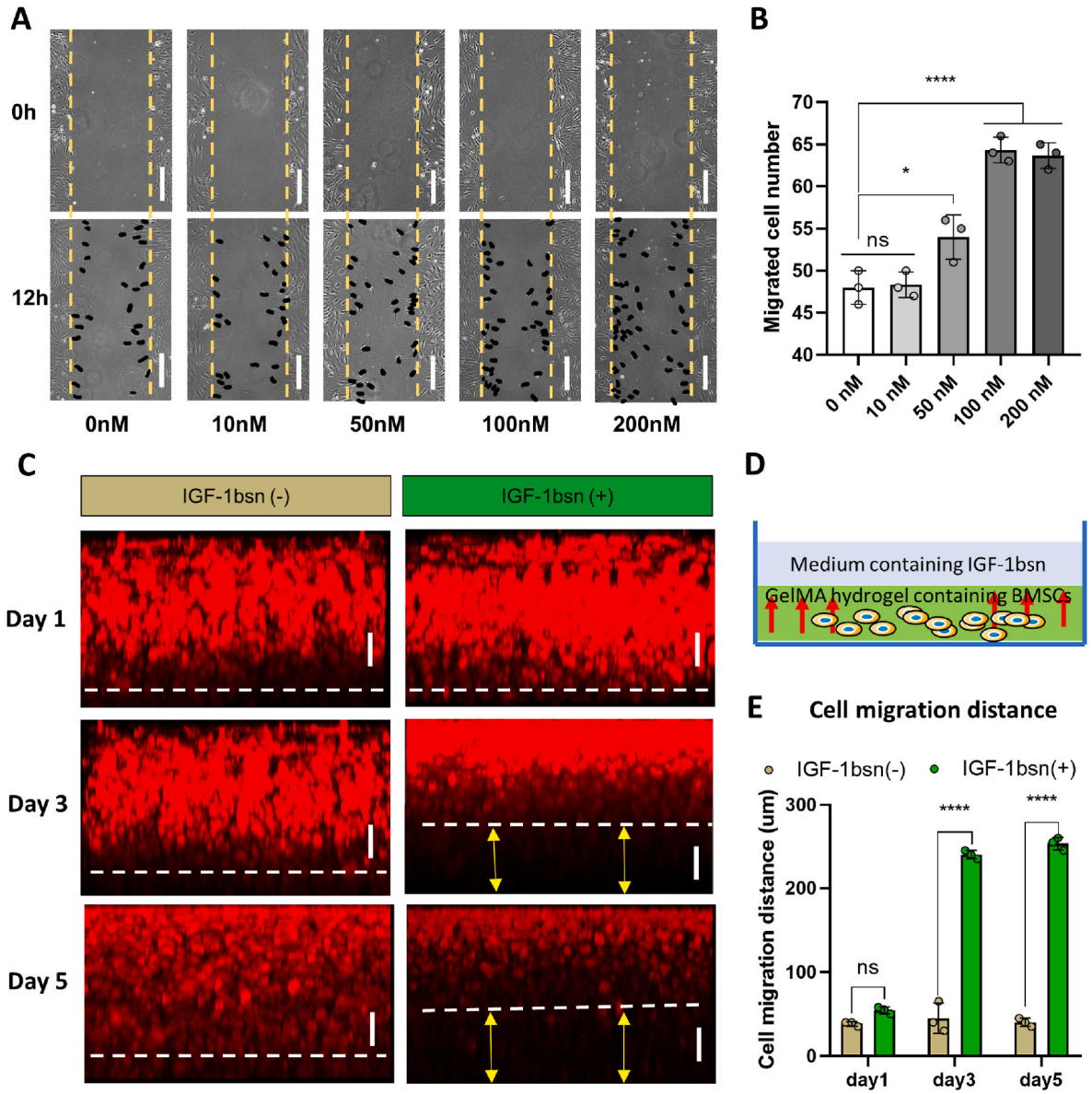

Fig. 2. IGF-1bsn promotes migration of BMSCs both in 2D and 3D culture conditions. (A) Representative images of the scratch test showing rabbit BMSCs immigration in 2D culture condition. Cells were treated with different concentrations of IGF-1bsn and 1% FBS for 24 h. Black dots indicated migrated cells. Scale bar = 100 μm. (B) Quantification analysis of the scratch test. n = 3 per group; ns: not significant; *$p < 0.05$, ****$p < 0.0001$. (C) Fluorescence images of cell migration in GelMA hydrogel on day 1, day 3, and day 5. The cell-hydrogel construct was cultured in medium with or without IGF-1bsn. Rabbit BMSCs were stained using phalloidin. Scale bar = 100 μm. (D) Schematic diagram of the cell migration assay. (E) Analysis of cell migration distance of BMSCs. n = 3 per group, ns: not significant, ****$p < 0.0001$.

45.0 ± 18.0 μm and 40.0 ± 5.0 μm, respectively, in control group (Fig. 2E). These data demonstrated that IGF-1bsn significantly enhanced migration of rBMSCs at a concentration of 200 nM *in vitro*.

3.4. IGF-1bsn inhibit apoptosis of BMSCs

To further demonstrate that IGF-1bsn could inhibit BMSC apoptosis, we used H_2O_2 to induce cell apoptosis and then rescued the cells using different doses of IGF-1bsn. Flow cytometry analysis revealed that the overall apoptosis proportion (top right corner + bottom right corner of the images) in the 200 nM group showed the lowest apoptosis rate (12.11 ± 1.67), which was significantly different from that of control group (24.92 ± 5.57) (Fig. 3A and B). The results of qRT-PCR further demonstrated apoptosis-related gene expression difference among each group. The expression level of *Bax* and *bad,* which are both pro-apoptotic genes, were down regulated in the 200 and 400 nM groups. The expression of *bcl2*, which plays a role in anti-apoptosis, was upregulated in the low-dose IGF-1bsn group, suggested that IGF-1bsn may inhibit cell apoptosis in low concentration (Fig. 3C). Based on the results of cell apoptosis, cell migration, and proliferation experiments, 100–200 nM IGF-1bsn was found to be the optimal range to promote cell proliferation and migration, and to inhibit cell apoptosis. Therefore, 100 times of this concentration (10 μM) was used in subsequent *in vivo* experiments.

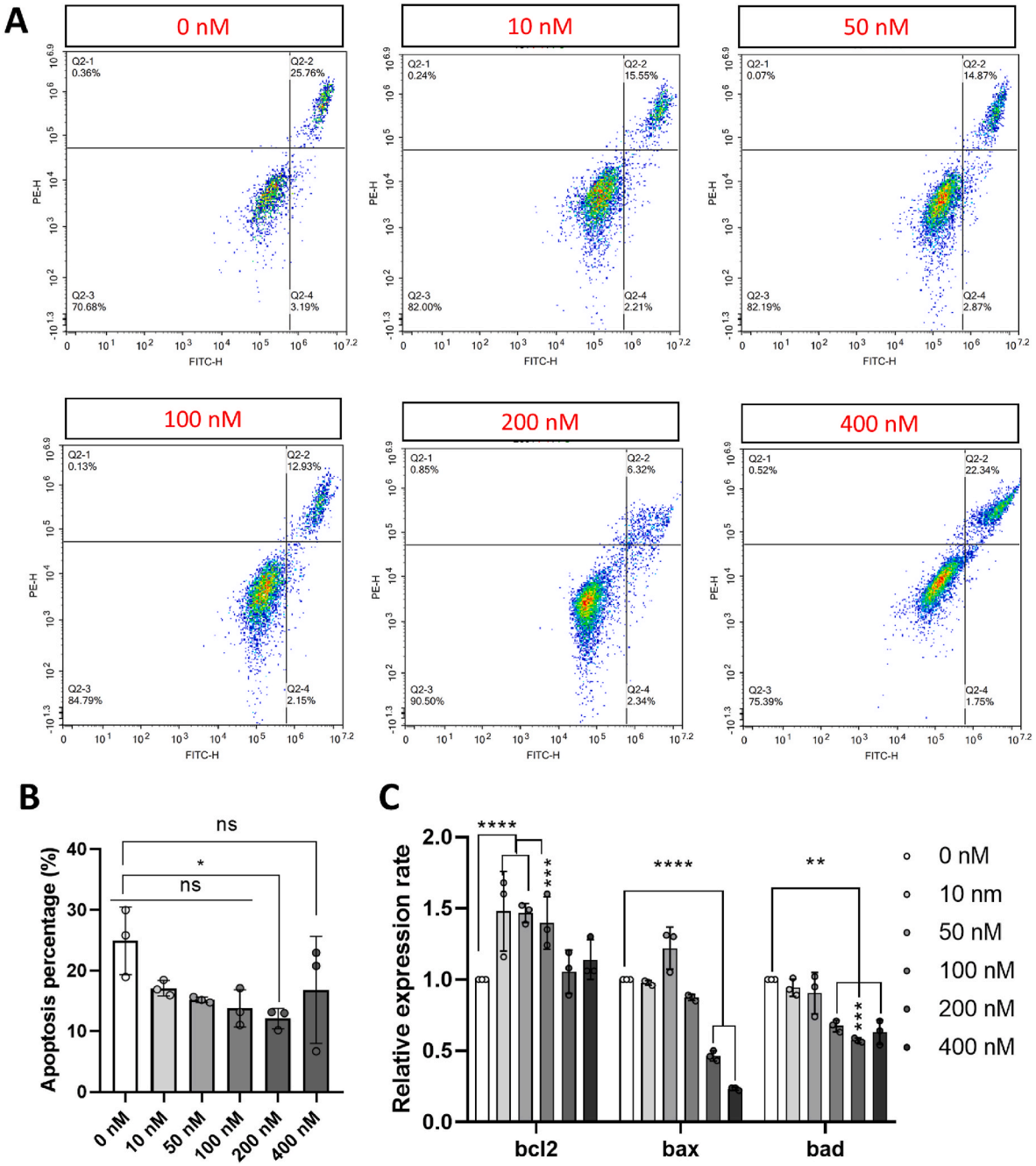

Fig. 3. IGF-1 bsn inhibit apoptosis of BMSCs. (A) Flow cytometry analysis of cell apoptosis of BMSCs cultured in medium containing different concentrations of IGF-1bsn (0–400 nM). (B) Quantification of apoptosis rate of BMSCs. (C) Real time PCR analysis of apoptosis related gene expression. Experiments repeated three times; n = 3 per group; ns: not significant; *p < 0.05, **p < 0.01, ****p < 0.0001.

3.5. Macroscopic evaluation shows efficacy of GelMA/IGF-1bsn hydrogel for osteochondral regeneration

The surgical procedure is shown in Fig. 4A. Post-operation macroscopic images displayed a smooth connection from the graft to the surrounding joint surface in the BSN-GelMA group at both 6 and 12 weeks, whereas the surgical gap in the blank group remained distinct and sunken, especially at 6 weeks (Fig. 4Bi and 4Ci). All the samples displayed a fibrous membrane on the surface of the joints, and the gaps in all groups became inconspicuous at 12 weeks (Fig. 4C). In accordance with the guidelines of the International Cartilage Repair Society (ICRS), the macroscope score results showed that there was a significant difference ($P < 0.001$) between the BSN-GelMA group (7.5 ± 0.33) and the blank group (4.25 ± 1.58) at both 6 and 12 weeks. A similar difference ($P < 0.05$) was observed between the BSN-GelMA and GelMA groups (Fig. 4D). However, the difference was diminished between each group at 12 weeks, indicating that the self-repair continued to function in the late stage.

Micro-CT scan images obtained from three-dimensional (3D) reconstruction, coronal view, and sagittal view were analyzed to evaluate the outcome of the gap interface. In the blank group, distinct gap around the graft and dense osteosclerosis in the graft were observed in the coronal and sagittal views (Fig. 5Ai and 5Bi). In the Gel and BSN-GelMA groups, the osseous gap around the graft was smaller. The percentage of osseous defects in the BSN-GelMA group ($43.29 \pm 8.98\%$) was much lower than that in the blank group ($57.87 \pm 13.12\%$) at 6 weeks ($P < 0.001$). At 12 weeks, this difference was even more pronounced in both Gel ($P < 0.001$) and BSN-GelMA ($P < 0.0001$) groups (Fig. 5C). However, there was no significant difference between the groups in terms of the ratio of bone volume to total volume (BV/TV) in the graft region (Fig. 5D). This was mainly because bone density and bone volume increased as bone sclerosis occurred in the blank group. On the other hand, the morphology of subchondral bone in BSN-GelMA group was close to normal bone with porous trabecular structure. This resulted that the bone density and bone volume was relatively close to the blank group. As seen in Fig. S7, the bone mineral density (BMD) showed that there was no difference among groups at 6 weeks. Hence the morphology of trabecular bone in the subchondral region is another factor influencing the value of BV/TV and Tb.Th. Trabecular thickness (Tb.Th) and trabecular separation (Tb.Sp) reflect the trabecular quality in each group. Although no difference was observed in Tb.Th values at 6 weeks, Tb.Sp was significantly lower in the BSN-GelMA group than in the blank group ($P < 0.01$). At 12 weeks, as the graft necrosis became stable and bone regeneration started, the trabecular spacing was comparable in each group (non-significant), but trabecular thickness showed the most significant increase in the BSN-GelMA group.

3.6. Histological staining proved early gap healing of osteochondral defect in BSN-GelMA group

Next, histology of the joint samples was analyzed using hematoxylin and eosin (H&E) staining, Safranin O-fast green staining, and Masson staining. Representative images showed obvious cracked fissures that persisted in the gap region of the bone in the blank group at 6 and 12 weeks. At 6 weeks, fibrotic tissue filled the gap and cancellous bone became sparse (Fig. 6Ai and 6Ci), indicating that bone absorbance occurred during this stage. This change was consistent with the Tb.Sp results obtained in the microCT analysis (Fig. 5F). At 12 weeks, the gap

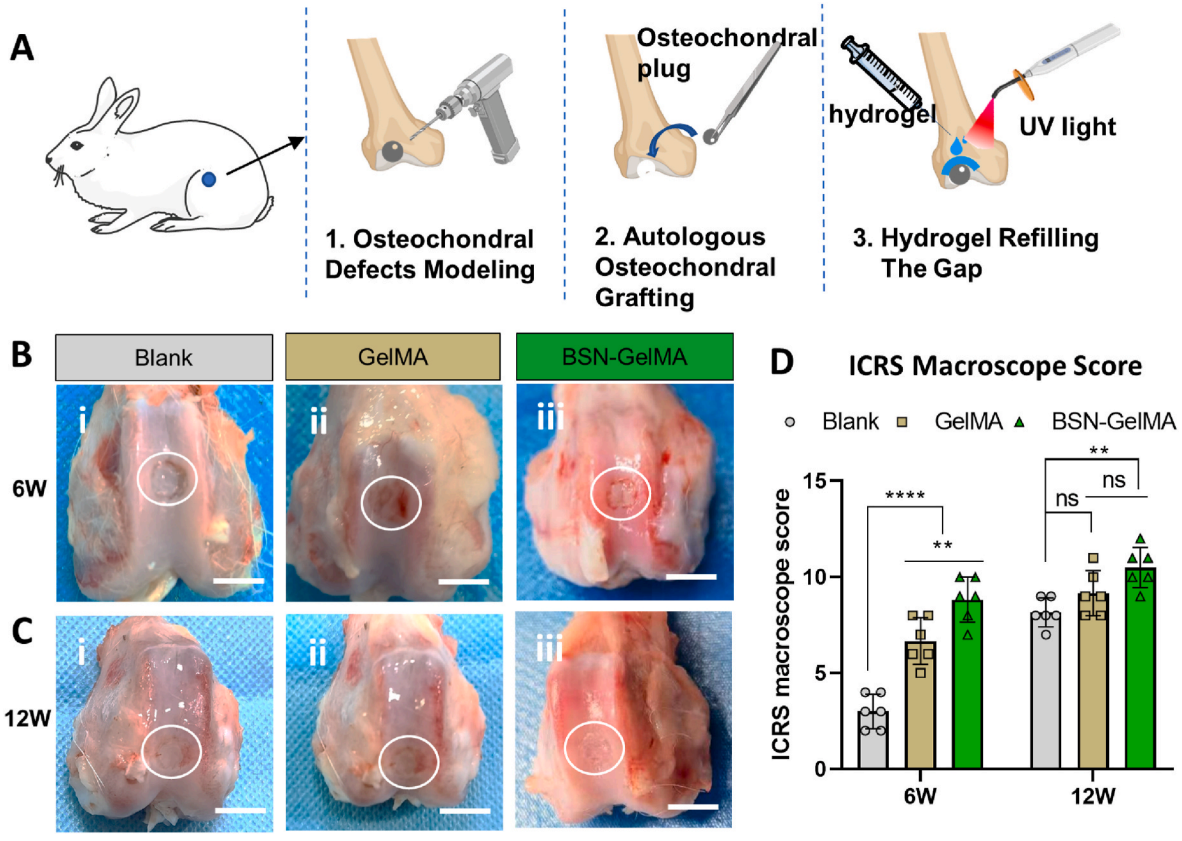

Fig. 4. Gross evaluation of the osteochondral repair by mosaicplasty surgery in a rabbit model. (A) Schematic diagram of the surgical procedure of the mosaic transplantation. Autologous osteochondral graft transplantation mimicking mosaicplasty is shown; the remaining gap was filled with GelMA hydrogel with or without IGF-1bsn, and any type of gel was not used to fill the gap in the blank group. (B) Gross view of the samples harvested 6 weeks post transplantation. (C) Gross view of the samples harvested 12 weeks post transplantation. (D) Analysis of ICRS score for the harvested samples. n = 6 per group; ns: not significant; *p < 0.05, **p < 0.01, ****p < 0.0001.

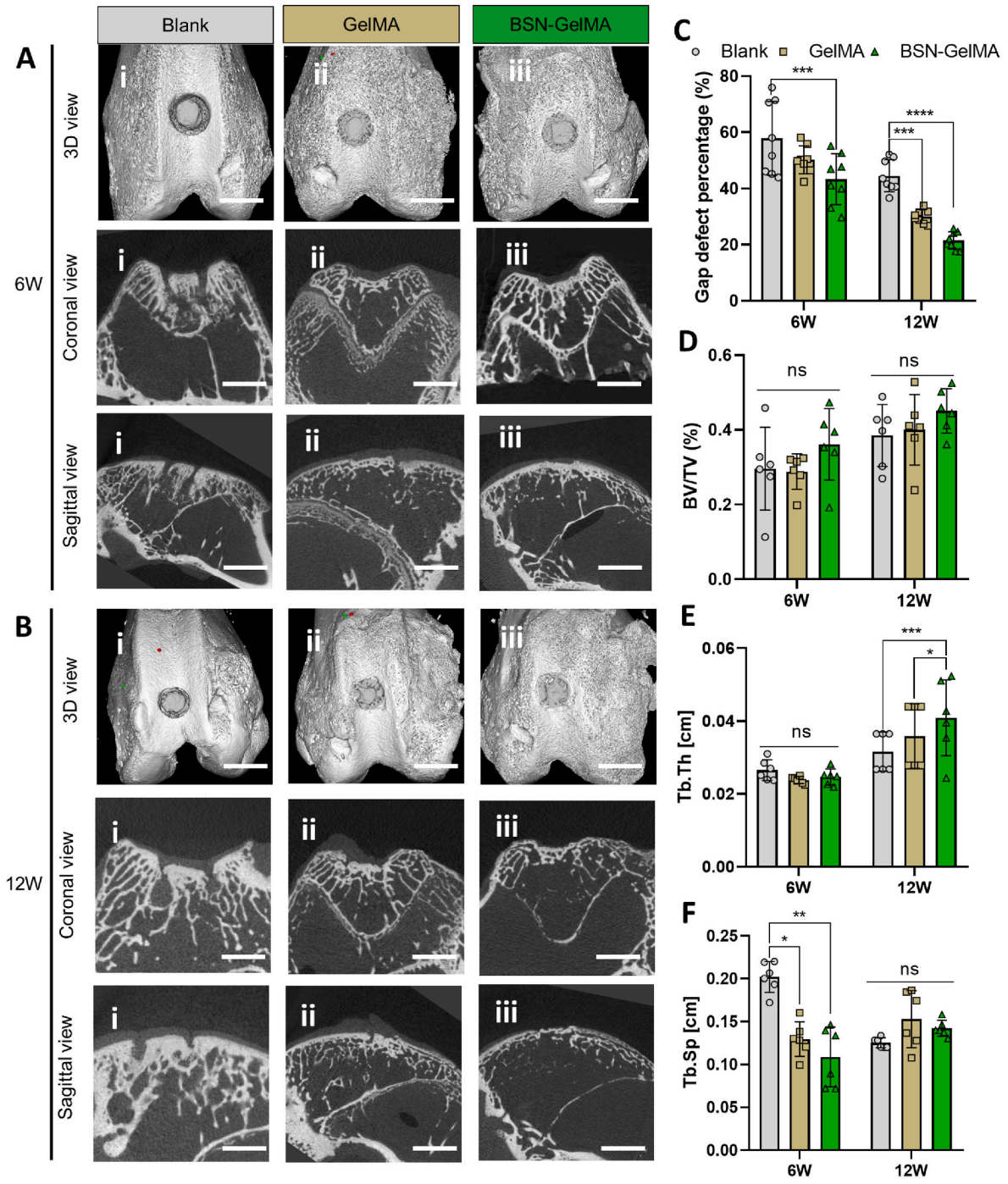

Fig. 5. Micro-computed tomography (micro-CT) analysis of rabbit femur osteoarticular bone. Representative 3D reconstructed image, coronal view, and sagittal view of each group at 6 weeks (A) and 12 weeks after mosaicplasty (B). (C) Quantitative analysis of defect area percentage in the gap between the host bone and graft, n = 8. (D) Quantitative analysis of bone volume to tissue volume (BV:TV). (E) Quantitative analysis of trabecular volume to thickness (Tb.Th). (F) Quantitative analysis of trabecular volume to spacing (Tb.Sp). n = 6 per group; ns: not significant; *p < 0.05, **p < 0.01, ***p < 0.001, ****p < 0.0001.

was still distinct, and cartilage tissue was observed even at the bottom of the gap. The subchondral region of the graft became compact, indicating the occurrence of osteosclerosis (Fig. 6Bi and 6Di). These findings were consistent with previously illustrated clinical problems, e.g., poor integration of the gap and generation of fibrous tissue. By contrast, the gap was filled with newly regenerated cartilage in the GelMA group at 6 weeks (Fig. 6 Aii and 6 Cii), and an almost normal osteochondral structure appeared with an intact edge in the gap interface in the BSN-GelMA group (Fig. 6Aiii and 6 Ciii). The histology score reflected the general evaluation of the quality of cartilage and subchondral bone in the defect region. The results suggested that the cartilage and subchondral scores in the BSN-GelMA group were the highest at all time points (Fig. 6E and F), which were significantly higher than those in the blank group ($P < 0.001$) and GelMA group ($P < 0.01$).

Safranin O-fast green (SF) staining revealed distribution of hyaline cartilage. Overall, the images at 6 weeks revealed that the apparent red staining in the gap region was only observed in the BSN-GelMA group (Fig. 6C–iii). The GelMA group displayed less mature cartilage and the blank group showed fibrotic tissue only (Fig. 6Ci and 6Cii). At 12 weeks, the difference among each group diminished, and the blank and GelMA

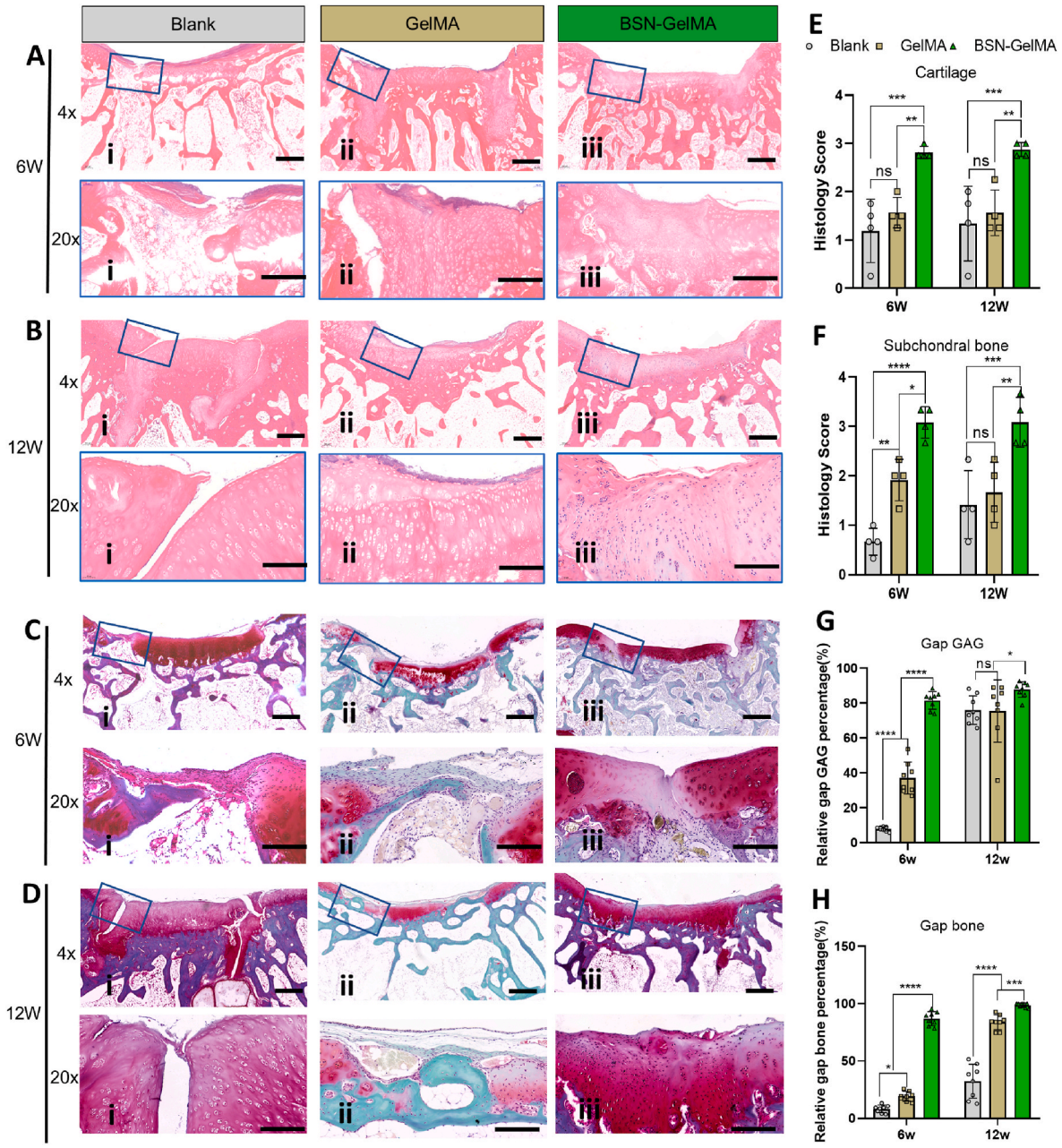

Fig. 6. Histological analysis of osteochondral regeneration at the transplantation site. Images of hematoxylin and eosin (H&E) stained samples at low and higher magnification (blue box) of each group at (A) week 6 and (B) week 12. Images of Safranin O and Fast green stained samples at low and higher magnification (blue box) of each group at (C) week 6 and (D) week 12. Scale bar 4x = 4 mm, 20x = 200 μm. (E) Evaluation of cartilage structure of the grafted bone at week 6 and week 12, n = 4. (F) Evaluation of subchondral bone formation in the gap surrounding the graft at week 6 and week 12, n = 4. (G) Evaluation of GAGs content of the gap surrounding the transplanted graft at week 6 and week 12 obtained from both sides of the graft, n = 8. (H) Evaluation of bone density of bone formed in the gap surrounding the transplanted graft at week 6 and week 12 obtained from both sides of the graft. n = 8; ns: not significant; *p < 0.05, **p < 0.01, ***p < 0.001, ****p < 0.0001.

groups displayed mature cartilage as well (Fig. 6D). To investigate the efficacy of regeneration of the bone in the gap region, we compared the gap GAG content in the cartilage layer and gap bone volume in the subchondral region obtained from both sides of the graft (Fig. 6G and H). Data revealed that relative GAG content and bone volume in BSN-GelMA group showed the highest value of 81.57 ± 5.05% (at 6 weeks) and 87.85 ± 4.46% (at 12 weeks), respectively, followed by that in GelMA group with 37.09 ± 9.14% (at 6 weeks) and 75.53 ± 17.87% (at 12 weeks) ($P < 0.0001$). These data suggested that IGF-1bsn played an important role in accelerating osteochondral regeneration. However, the difference among each group diminished at 12 weeks, especially in the GAG content. This result indicates that the blank group underwent a slower self-regeneration process than the BSN-GelMA group. By contrast, the different GAG content suggested that more fibrous tissues and fibrocartilage was generated in the blank group than in the BSN-GelMA group. These data implies that the addition of the hydrogel was able to prevent the formation of fibrous tissues as well as to preserve hyaline cartilage viability.

Furthermore, Masson's staining was performed to validate the subchondral bone regeneration. Images at 6 weeks demonstrated that distinct cancellous bone was distributed throughout the gap region in the BSN-GelMA group (Fig. 7C). However, a large amount of cartilage

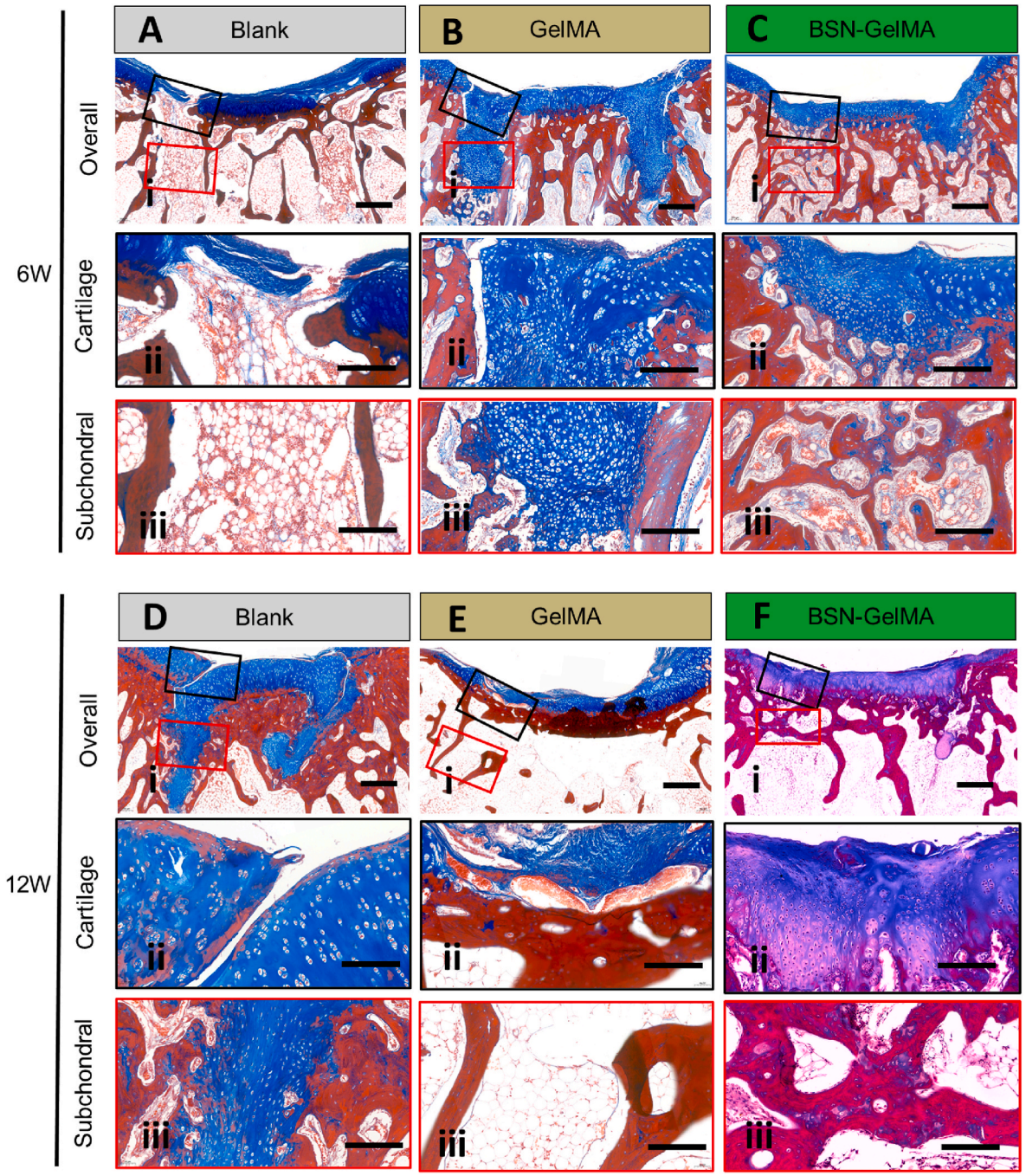

Fig. 7. Images of Masson's trichrome-stained samples showing a gap region at 6 (A, B, C) and 12 (D, E, F) weeks in each group. A and D: Blank group, B and E: GelMA group, C and F: BSN-GelMA group. i: overall view of the graft region. ii: cartilage layer in the gap region (blue square); iii: subchondral layer in the gap region (red square). Scale bar: i = 4 mm, ii and iii = 200 μm.

appeared in the gap region of the GelMA group, whereas only fibrous tissue was found in that of the blank group (Fig. 7A-B). At 12 weeks, a large quantity of cartilage appeared in the gap of the blank group, and a gap was not seen in BSN-GelMA and BSN-GelMA groups (Fig. 7D-F). The results further demonstrated that osteochondral regeneration in the gap region of BSN-GelMA group started much earlier than in the GelMA and blank groups.

3.7. IGF-1bsn preserves cartilage viability of the graft

To investigate the hyaline cartilage distribution in the gap region and preservation in the graft, immunofluorescence of collagen II in hyaline cartilage was performed. The expression level of collagen II in the gap regions of the GelMA group (1.68 ± 0.08, $P < 0.001$) and BSN-GelMA group (2.50 ± 0.12, $P < 0.0001$) was significantly higher than that in the blank group at both 6 weeks and 12 weeks (Fig. 8E-F), indicating that hydrogel could promote the cartilage regeneration after mosaicplasty. And the addition of IGF-1bsn in the hydrogel could further accelerate the regeneration by comparing with the hydrogel only ($P < 0.001$, Fig. 8E-F). Interestingly, collagen II expression in the graft region displayed similar trends at the two time points (Fig. 8G-H). The expression level of collagen II in BSN-GelMA group was the highest at both 6 weeks (2.14 ± 0.07) and 12 weeks (2.06 ± 0.04), followed by GelMA group (1.80 ± 0.06 and 1.49 ± 0.06, respectively). The blank

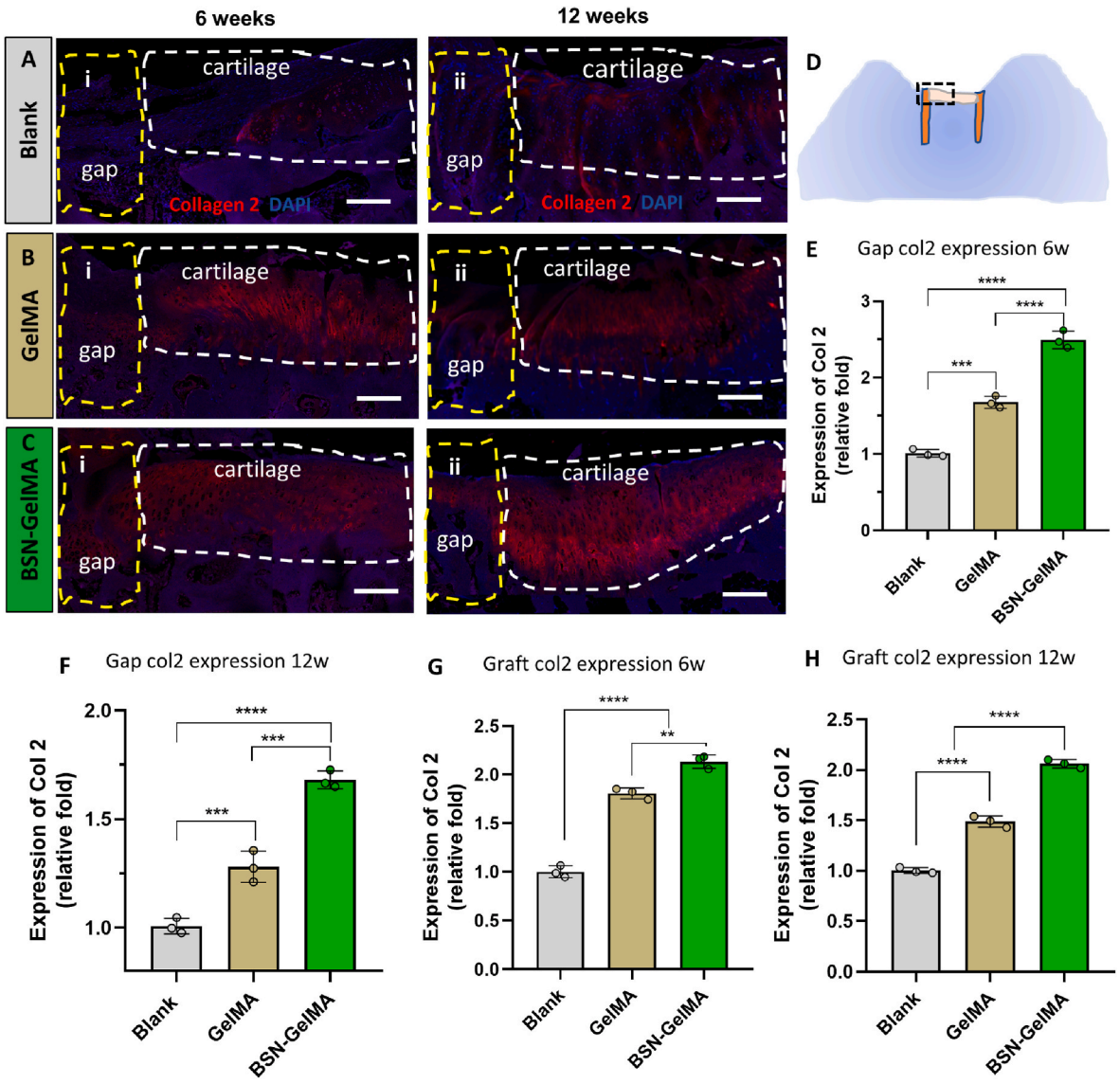

Fig. 8. Analysis of collagen II expression in the graft at weeks 6 and 12 after surgery. Immunofluorescence staining of Collagen II at 6 and 12 weeks in (A) blank group, (B) GelMA group, and (C) BSN-GelMA group. White dotted lines indicate the cartilage region of the transplanted osteochondral graft; Yellow dotted lines indicate the gap region adjacent to the graft. (D) Schematic graph showing the histology of an osteochondral slice; black dashed frame indicates the region taken for collagen II evaluation. Relative expression level of collagen II in the gap region (E and F) and cartilage region (G and H) of the graft at 6 and 12 weeks, respectively. Scale bar = 200 μm n = 3 per group; ns: not significant; *p < 0.05, **p < 0.01, ***p < 0.001, ****p < 0.0001.

group showed the lowest intensity of staining (P < 0.0001) (Fig. 8G-H). The viability of the cartilage in the graft was adequately preserved, which was beneficial for graft survival after mosaicplasty. Similarly, Tunel staining of the specimens at 6 weeks showed that the overall apoptosis rate in blank group was the highest (P < 0.01) And there was no significant difference between GelMA and BSN-GelMA group (Fig. S8).

4. Discussion

In the present study, we compared an effective strategy by accelerating gap integration after mosaicplasty with a conventional surgical approach (Fig. 9A). The untreated mosaicplasty group displayed poor gap integration and had complications such as, cyst formation, fibrous cartilage formation, subchondral necrosis, and osteosclerosis (Fig. 9B and C). By contrast, significantly earlier and seamless osteochondral healing was accomplished in the BSN-GelMA group than in the untreated group because the bone space was filled with IGF-1 bioactive supramolecular nanofibers (Fig. 9D-F). IGF-1 bioactive supramolecular nanofibers incorporated hydrogel acted as a tissue filler to bridge the gap, prevent cartilage degeneration, and promote graft survival and BMSC migration (Fig. 9G). Thus, this strategy may have strong implications for cell-free therapy in *in situ* tissue regeneration.

From the above-mentioned data, the gap of blank group remained distinct even at 12 weeks, indicating poor tissue regeneration and gap integration. This is different from the previous reports that there is high spontaneous recovery rate in many preclinical animal models [55,56]. The expression of collagen II in the graft region of blank group diminished, suggesting that the cartilage of the graft underwent degradation and fibrotic changes. The expression of collagen II was also low in the gap region, suggesting that regeneration of the cartilage was weak. Gulotta et al. reported that necrosis, apoptosis, and matrix degradation of chondrocytes occurred after press-fit osteochondral autograft implantation in a rabbit model [14]. This result is consistent with that in our study. Interestingly, in our study, from the histological images in the blank group, it was found that two cases at 12 weeks showed a distinct

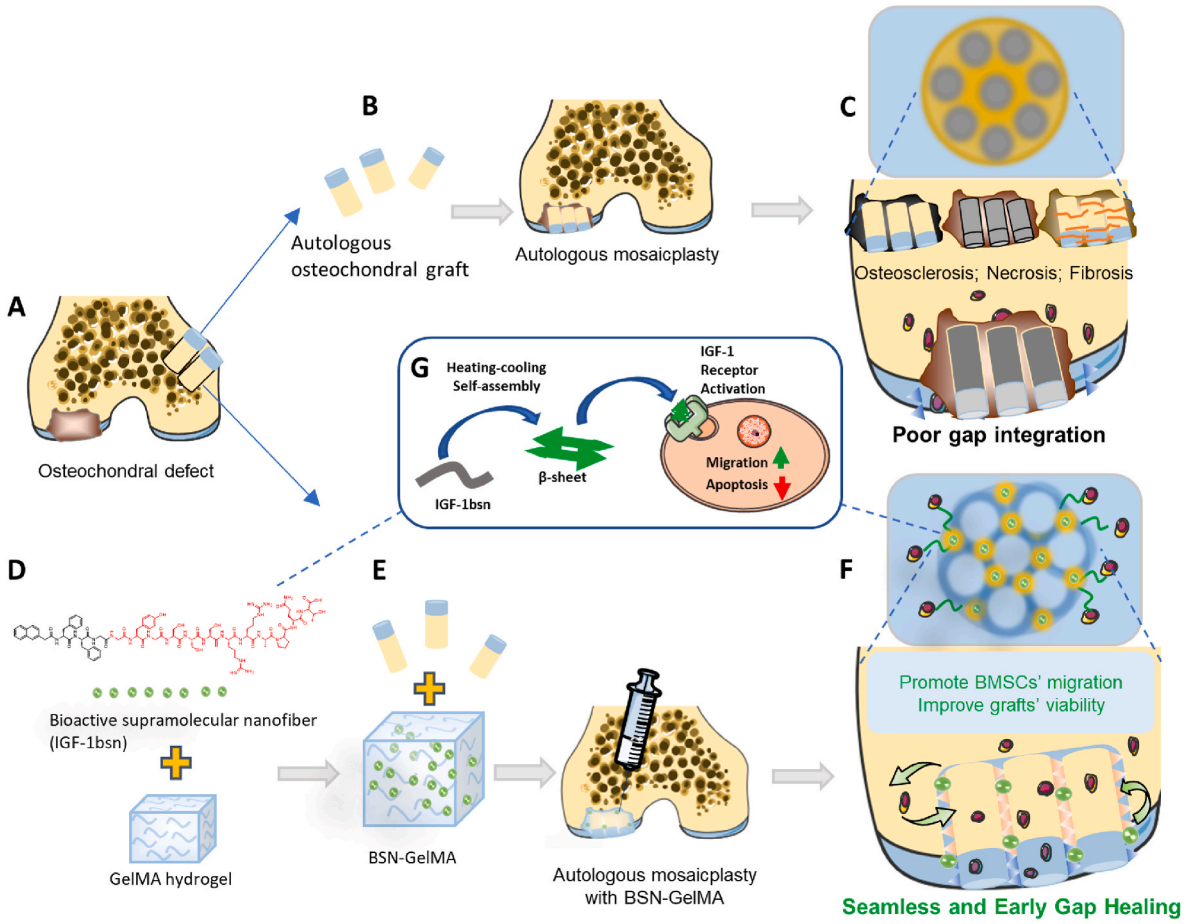

Fig. 9. Schematic diagram of the IGF-1bsn functioning as activators for promoting cell proliferation and inhibiting apoptosis. (A) An osteochondral defect in the distal femoral trochlear bone. (B) The osteochondral defect was treated using a conventional autologous mosaicplasty. (C) Common complications caused by the conventional autologous mosaicplasty. (D and E) The osteochondral defect was treated using autologous mosaicplasty together with GelMA hydrogel containing IGF-1bsn. (F) The IGF-1bsn enhance seamless and early healing of osteochondral graft by promoting migration of BMSCs and graft viability. (G) IGF-1bsn influences cell behavior by activating the IGF-1 receptor pathway.

rivet shape of newly formed cartilage tissue in the gap from the bottom to the top area, with distinct fissures but relatively high GAG content. In addition, cyst formation, which is considered to be the most widely reported bone change after trauma or surgery, was observed in the cartilage tissue section [57]. We were interested in knowing the reason as to why these cartilage tissues were not ossified at this time point and whether they were likely to ossify in the future. Previous studies reported that an irregular subchondral architecture might cause progression of cartilage defects in osteoarthritis or osteochondral defects, based on long-term observations in patients after microfracture or debridement [58]. Subchondral bone plates have been found to have a distinct chronological arrangement, and a relevant alteration may affect upward migration and even cartilage regeneration [59], suggesting that integrity of bone tissues and appropriate development in the grafted bone might be fundamental for growth of the upper layer. In addition, progressive subchondral bone thickening was reported to induce chondrocyte apoptosis and hyaline cartilage degradation in osteoarthritis [60]. A report suggested that better osteochondral defect repair could be achieved by restoration of the subchondral bone integrity using a novel surgical technique [61]. Thus, successful repair of subchondral bone, but not aggressive osseous development, is essential for overall osteochondral defect repair. Hence, we speculate that newly formed cartilage might impede subchondral bone regeneration, and the gap may not be able to integrate even after a long time.

By contrast, the GelMA group showed superior tissue regeneration capacity than blank group, indicating that the hydrogel promoted plug integration and osteochondral regeneration in the gap region. Moreover, GelMA hydrogel has superior biocompatibility and biodegradation capacity, and can be hybridized with other biomimetic materials such as biopolymers, nanoparticles, and organic factors to display combined advantages [62–65]. However, the images of SF and collagen II staining in the gap area of the GelMA group showed scattered hyaline cartilage appearance, indicating that the quality of regenerated tissue was not satisfactory at this time point. This result implied that the GelMA hydrogel alone was not sufficient to induce efficient in situ osteochondral regeneration. In previous studies, allogeneic BMSCs containing pure Pluronic F-127 hydrogel were reported to be able to repair osteochondral defects and integrate the "dead space" in a rabbit model [21]. However, allogeneic cells are at risk of immune rejection and disease transmission, which is not acceptable to all patients. Therefore, supramolecular nanofibers formed by self-assembly of customized peptides, which possess a bioactive potential similar to natural growth factors, may provide a more powerful solution to promote tissue regeneration [66].

Surprisingly, the BSN-GelMA group exhibited the fastest osteochondral regeneration, as early as 6 weeks, suggesting that the addition of IGF-1bsn was effective in promoting gap integration and graft survival. SF and collagen II staining demonstrated that obvious hyaline cartilage regeneration in the gap region, with fully seamless subchondral regeneration. Besides, the ICRS score, histology score, collagen II expression level, and gap GAG and subchondral bone content were the highest among all the groups. Furthermore, the GelMA/IGF-1bsn

hydrogel possessed a superior regeneration capacity to expedite gap integration and tissue regeneration.

As observed from *in vitro* experimental results, several aspects related to the functioning of IGF-1bsn to promote tissue regeneration may be considered. Firstly, IGF-1bsn played an active role in enhancing BMSCs' proliferation. Unlike previous studies, IGF-1bsn did not activate BMSCs' proliferation until day 5, even at 0% FBS. However, this effect was more significant in other cell types than in BMSCs [40]. It is worth noting that, in the cell scratch assay, BMSCs also exhibited a strong migration and invasion activity without the addition of FBS. This finding is beneficial for the application of serum-free culture media, which is more suitable for clinical use [67]. Bioactive supramolecular nanofibers, because of their structural diversity, usually play multiple functions in promoting cell proliferation, migration, differentiation, etc. [26,28,39]. However, the effects may vary in different cell types and disease conditions. IGF-1bsn has been shown to inhibit a variety of disorders, including ischemic limb disease, sarcopenia, acute kidney injury, and atherosclerosis [40,42,68,69]. However, to the best of our knowledge this study is the first to report the positive effect of IGF-1 bsn on gap integration after mosaicplasty in osteochondral defect therapy.

Secondly, the IGF-1bsn peptide showed a strong anti-apoptotic effect. In addition to the *in vitro* experimental data, collagen II staining *in vivo* demonstrated that hyaline cartilage degeneration was more obvious in the blank group than in BSN-GelMA group. This result suggested that the graft viability was protected by the composite hydrogel through bridging of the graft with the host bone. This effect was mainly due to the internal structure of bioactive signals that bind to the cell receptor of IGF-1 [40]. It has been reported that the functions and viability of chondrocytes are critical to maintain a maximum volume of extracellular matrix and ensure long-term graft survival [16,17]. To verify the apoptosis rate of the graft, we performed immunohistochemical staining for Tunel at 6 weeks. The semi-quantitative statistical result showed that the overall apoptosis rate in blank group was the highest ($P < 0.01$, Fig. S7).

Thirdly and importantly, IGF-1bsn promoted migration of BMSCs. After bridging the plug with the host bone using a composite hydrogel, it is important to recruit host stem cells to the gap region and initiate the regeneration process [70], especially in the early stage after transplantation. In the *in vitro* experiment, a significant difference of cell migration was observed. However, how bioactive materials recruit stem cells from host tissue to the defect area is still unknown cells' migration *in vivo* [71,72]. It's well known that some natural chemokine such as interleukin 8 (IL-8) and stromal cell-derived factor-1α (SDF-1α) could promote BMSCs' migration [73–77]. IGF-1 is commonly accepted that it could enhance the BMSCs' migration and chondrogenic growth [78–80]. Accumulative previous studies revealed that the repairing process begins with host stem cell influx, which often occurs in less than 1 week post implantation [81]. However, cell migration is governed by various conditions, thus making it difficult to study in native environments [82]. Firstly, it requires the cell to squeeze through dense or complex extracellular structures through 3D environments, which requires specific cellular adaptations or remodeling to mechanical features of the extracellular matrix (ECM) [83]. Secondly, cells in 3D environment in *vivo* often interact with neighboring cells and tissues through physical and signaling interactions, which need to overcome extracellular barriers and stiffness [84]. Therefore, enhancement of cell migration may be only one aspect attributing to the superior regeneration capacity of GelMA-IGF-1bsn.

In our study, despite the prominent effect of IGF-1bsn in promoting osteochondral regeneration, it is worth noting that subtle fissures still existed in some gap regions of the BSN-GelMA group, even at 12 weeks, suggesting that there might be other factors impeding cartilage integration. It has been reported that even adjacent cartilages may be difficult to fuse together because of the proteoglycan nature of the main components of the cartilage matrix. Proteoglycans have anti-adhesion properties, which can hinder the fusion of proteoglycans in adjacent cartilage tissue, thus affecting healing between two grafts [10]. Thus, interaction of IGF-1bsn with the ECM of cartilage may warrant further investigation. Moreover, the effects of IGF-1bsn on BMSCs in terms of proangiogenic, osteogenic, and chondrogenic capacities, which might be other contributing factors to promote tissue regeneration, should also be investigated in the future.

5. Conclusion

In summary, to the best of our knowledge, this study is the first to investigate the effects of an injectable IGF-1 bioactive supramolecular nanofiber-enabled GelMA hydrogel (BSN-GelMA) that can accelerate gap integration between osteochondral plugs and surrounding tissues after mosaicplasty, which ultimately facilitate the repair outcome. With high biocompatibility, stable activity, and low cost, IGF-1bsn is superior to natural IGF-1 protein and significantly promotes migration and viability of BMSCs *in vitro*, as well as promotes cell proliferation in a restrained manner. As a result, BSN-GelMA promotes space integration, and primarily results in early subchondral regeneration and subsequent cartilage regeneration to protect the graft from degeneration. The application of bioactive synthetic agents to common biocompatible hydrogels provides new insights into the strategies used to perform osteochondral mosaicplasty. Therefore, we propose a promising off-the-shelf bioactive material for cell-free in situ tissue regeneration.

CRediT authorship contribution statement

Hongwei Wu: Data curation, Methodology, Writing – original draft. **Yuna Shang:** Formal analysis, Methodology, Resources, Validation, Writing – review & editing. **Wei Sun:** Data curation. **Xinyi Ouyang:** Data curation. **Wenyan Zhou:** Data curation. **Jieji Lu:** Data curation, Writing – original draft. **Shuhui Yang:** Data curation, Writing – original draft. **Wei Wei:** Data curation. **Xudong Yao:** Writing – review & editing. **Xiaozhao Wang:** Writing – review & editing. **Xianzhu Zhang:** Data curation. **Yishan Chen:** Writing – review & editing. **Qiulin He:** Writing – review & editing. **Zhimou Yang:** Resources, Writing – review & editing. **Hongwei Ouyang:** Conceptualization, Funding acquisition, Project administration, Resources, Supervision, Validation, Visualization, Writing – review & editing.

Declaration of competing interest

All the authors declared that there was no conflict of interest regarding to this study. There was no competing financial interest related to this study as well.

Acknowledgements

This work is supported by the National Key Research and Development Program of China (2016YFB0700804) and National Natural Science Foundation of China (NO. T2121004, 31830029).

Appendix A. Supplementary data

Supplementary data to this article can be found online at https://doi.org/10.1016/j.bioactmat.2022.03.038.

References

[1] E.B. Hunziker, K. Lippuner, M.J. Keel, N. Shintani, An educational review of cartilage repair: precepts & practice–myths & misconceptions–progress & prospects, Osteoarthritis Cartilage 23 (3) (2015) 334–350.
[2] L. Bartha, A. Vajda, Z. Duska, H. Rahmeh, L. Hangody, Autologous osteochondral mosaicplasty grafting, J. Orthop. Sports Phys. Ther. 36 (10) (2006) 739–750.
[3] C. Ai, Y.H.D. Lee, X.H. Tan, S.H.S. Tan, J.H.P. Hui, J.C. Goh, Osteochondral tissue engineering: perspectives for clinical application and preclinical development, J Orthop Translat 30 (2021) 93–102.

[4] A. Sabaghzadeh, F. Mirzaee, H. Shahriari Rad, F. Bahramian, A. Alidousti, H. Aslani, Osteochondral autograft transfer (mosaicplasty) for treatment of patients with osteochondral lesions of talus, Chin. J. Traumatol. 23 (1) (2020) 60–62.

[5] G. Jacob, K. Shimomura, N. Nakamura, Osteochondral injury, management and tissue engineering approaches, Front. Cell Dev. Biol. 8 (2020), 580868.

[6] L. Hangody, G. Vasarhelyi, L.R. Hangody, Z. Sukosd, G. Tibay, L. Bartha, G. Bodo, Autologous osteochondral grafting–technique and long-term results, Injury 39 (Suppl 1) (2008) S32–S39.

[7] S. Banerjee, K.S. Sahanand, Managing chondral lesions: a literature review and evidence-based clinical guidelines, Indian J. Orthop. 55 (2) (2021) 252–262.

[8] L. Hangody, G. Kish, T. Koreny, L.R. Hangody, L. Módis, 8 - cartilage tissue repair: autologous osteochondral mosaicplasty, in: C. Archer, J. Ralphs (Eds.), Regenerative Medicine and Biomaterials for the Repair of Connective Tissues, Woodhead Publishing, 2010, pp. 201–226.

[9] M.F. Erol, O. Karakoyun, A new point of view for mosaicplasty in the treatment of focal cartilage defects of knee joint: honeycomb pattern, SpringerPlus 5 (1) (2016) 1170.

[10] A. Bedi, B.T. Feeley, R.J. Williams 3rd, Management of articular cartilage defects of the knee, J. Bone Joint Surg. Am. 92 (4) (2010) 994–1009.

[11] J.G. Lane, J.B. Massie, S.T. Ball, M.E. Amiel, A.C. Chen, W.C. Bae, R.L. Sah, D. Amiel, Follow-up of osteochondral plug transfers in a goat model: a 6-month study, Am. J. Sports Med. 32 (6) (2004) 1440–1450.

[12] C.O. Tibesku, T. Szuwart, T.O. Kleffner, P.M. Schlegel, U.R. Jahn, H. Van Aken, S. Fuchs, Hyaline cartilage degenerates after autologous osteochondral transplantation, J. Orthop. Res. 22 (6) (2004) 1210–1214.

[13] T. Rose, S. Craatz, P. Hepp, C. Raczynski, J. Weiss, C. Josten, H. Lill, The autologous osteochondral transplantation of the knee: clinical results, radiographic findings and histological aspects, Arch. Orthop. Trauma Surg. 125 (9) (2005) 628–637.

[14] L.V. Gulotta, J.R. Rudzki, D. Kovacevic, C.C. Chen, D. Milentijevic, R. J. Williams 3rd, Chondrocyte death and cartilage degradation after autologous osteochondral transplantation surgery in a rabbit model, Am. J. Sports Med. 37 (7) (2009) 1324–1333.

[15] A. Bakay, L. Csonge, G. Papp, L. Fekete, Osteochondral resurfacing of the knee joint with allograft. Clinical analysis of 33 cases, Int. Orthop. 22 (5) (1998) 277–281.

[16] R.S. Gilmore, A.J. Palfrey, A histological study of human femoral condylar articular cartilage, J. Anat. 155 (1987) 77–85.

[17] R.S. Gilmore, A.J. Palfrey, Chondrocyte distribution in the articular cartilage of human femoral condyles, J. Anat. 157 (1988) 23–31.

[18] P. Duan, Z. Pan, L. Cao, J. Gao, H. Yao, X. Liu, R. Guo, X. Liang, J. Dong, J. Ding, Restoration of osteochondral defects by implanting bilayered poly(lactide-co-glycolide) porous scaffolds in rabbit joints for 12 and 24 weeks, J Orthop Translat 19 (2019) 68–80.

[19] L. Galois, A.M. Freyria, L. Grossin, P. Hubert, D. Mainard, D. Herbage, J.F. Stoltz, P. Netter, E. Dellacherie, E. Payan, Cartilage repair: surgical techniques and tissue engineering using polysaccharide- and collagen-based biomaterials, Biorheology 41 (3–4) (2004) 433–443.

[20] N. Iwasaki, H. Kato, J. Ishikawa, T. Masuko, T. Funakoshi, A. Minami, Autologous osteochondral mosaicplasty for osteochondritis dissecans of the elbow in teenage athletes, J. Bone Joint Surg. Am. 91 (10) (2009) 2359–2366.

[21] X. Ma, Y. Sun, X. Cheng, Y. Gao, B. Hu, G. Wen, Y. Qian, W. Gu, Y. Mao, W. Liu, Repair of osteochondral defects by mosaicplasty and allogeneic BMSCs transplantation, Int. J. Clin. Exp. Med. 8 (4) (2015) 6053–6059.

[22] T. Funakoshi, D. Momma, Y. Matsui, T. Kamishima, Y. Matsui, D. Kawamura, Y. Nagano, N. Iwasaki, Autologous osteochondral mosaicplasty for centrally and laterally located, advanced capitellar osteochondritis dissecans in teenage athletes: clinical outcomes, radiography, and magnetic resonance imaging findings, Am. J. Sports Med. 46 (8) (2018) 1943–1951.

[23] T.Y. Emre, Z. Atbasi, D.T. Demircioglu, M. Uzun, O. Kose, Autologous osteochondral transplantation (mosaicplasty) in articular cartilage defects of the patellofemoral joint: retrospective analysis of 33 cases, Musculoskel. Surg. 101 (2) (2017) 133–138.

[24] L. Chadli, J. Cottalorda, M. Delpont, P. Mazeau, Y. Thouvenin, D. Louahem, Autologous osteochondral mosaicplasty in osteochondritis dissecans of the patella in adolescents, Int. Orthop. 41 (1) (2017) 197–202.

[25] A. Clave, J.F. Potel, E. Servien, P. Neyret, F. Dubrana, E. Stindel, Third-generation autologous chondrocyte implantation versus mosaicplasty for knee cartilage injury: 2-year randomized trial, J. Orthop. Res. 34 (4) (2016) 658–665.

[26] X. Yan, Y.R. Chen, Y.F. Song, J. Ye, M. Yang, B.B. Xu, J.Y. Zhang, X. Wang, J.K. Yu, Advances in the application of supramolecular hydrogels for stem cell delivery and cartilage tissue engineering, Front. Bioeng. Biotechnol. 8 (2020) 847.

[27] C.H. Chen, E.L. Hsu, S.I. Stupp, Supramolecular self-assembling peptides to deliver bone morphogenetic proteins for skeletal regeneration, Bone 141 (2020), 115565.

[28] J. Xu, Q. Feng, S. Lin, W. Yuan, R. Li, J. Li, K. Wei, X. Chen, K. Zhang, Y. Yang, T. Wu, B. Wang, M. Zhu, R. Guo, G. Li, L. Bian, Injectable stem cell-laden supramolecular hydrogels enhance in situ osteochondral regeneration via the sustained co-delivery of hydrophilic and hydrophobic chondrogenic molecules, Biomaterials 210 (2019) 51–61.

[29] H. Cho, J. Kim, S. Kim, Y.C. Jung, Y. Wang, B.J. Kang, K. Kim, Dual delivery of stem cells and insulin-like growth factor-1 in coacervate-embedded composite hydrogels for enhanced cartilage regeneration in osteochondral defects, J. Contr. Release 327 (2020) 284–295.

[30] K. Kim, J. Lam, S. Lu, P.P. Spicer, A. Lueckgen, Y. Tabata, M.E. Wong, J.A. Jansen, A.G. Mikos, F.K. Kasper, Osteochondral tissue regeneration using a bilayered composite hydrogel with modulating dual growth factor release kinetics in a rabbit model, J. Contr. Release 168 (2) (2013) 166–178.

[31] M.R. Jung, I.K. Shim, H.J. Chung, H.R. Lee, Y.J. Park, M.C. Lee, Y. Il Yang, S.H. Do, S.J. Lee, Local BMP-7 release from a PLGA scaffolding-matrix for the repair of osteochondral defects in rabbits, J. Contr. Release 162 (3) (2012) 485–491.

[32] J. Nakayama, H. Fujioka, I. Nagura, T. Kokubu, T. Makino, R. Kuroda, Y. Tabata, M. Kurosaka, The effect of fibroblast growth factor-2 on autologous osteochondral transplantation, Int. Orthop. 33 (1) (2009) 275–280.

[33] R. Reyes, A. Delgado, E. Sanchez, A. Fernandez, A. Hernandez, C. Evora, Repair of an osteochondral defect by sustained delivery of BMP-2 or TGFbeta1 from a bilayered alginate-PLGA scaffold, J. Tissue Eng. Regen. Med. 8 (7) (2014) 521–533.

[34] C. Alemdar, I. Yucel, B. Erbil, H. Erdem, R. Atic, E. Ozkul, Effect of insulin-like growth factor-1 and hyaluronic acid in experimentally produced osteochondral defects in rats, Indian J. Orthop. 50 (4) (2016) 414–420.

[35] J.A. Lewis, R. Freeman, J.K. Carrow, T.D. Clemons, L.C. Palmer, S.I. Stupp, Transforming growth factor beta-1 binding by peptide amphiphile hydrogels, ACS Biomater. Sci. Eng. 6 (8) (2020) 4551–4560.

[36] H. Shigemitsu, T. Fujisaku, W. Tanaka, R. Kubota, S. Minami, K. Urayama, I. Hamachi, An adaptive supramolecular hydrogel comprising self-sorting double nanofibre networks, Nat. Nanotechnol. 13 (2) (2018) 165–172.

[37] M.P. Hendricks, K. Sato, L.C. Palmer, S.I. Stupp, Supramolecular assembly of peptide amphiphiles, Acc. Chem. Res. 50 (10) (2017) 2440–2448.

[38] A. Mershin, B. Cook, L. Kaiser, S. Zhang, A classic assembly of nanobiomaterials, Nat. Biotechnol. 23 (11) (2005) 1379–1380.

[39] M.J. Webber, J. Tongers, C.J. Newcomb, K.T. Marquardt, J. Bauersachs, D. W. Losordo, S.I. Stupp, Supramolecular nanostructures that mimic VEGF as a strategy for ischemic tissue repair, Proc. Natl. Acad. Sci. U. S. A. 108 (33) (2011) 13438–13443.

[40] Y. Shang, D. Zhi, G. Feng, Z. Wang, D. Mao, S. Guo, R. Liu, L. Liu, S. Zhang, S. Sun, K. Wang, D. Kong, J. Gao, Z. Yang, Supramolecular nanofibers with superior bioactivity to insulin-like growth factor-I, Nano Lett. 19 (3) (2019) 1560–1569.

[41] Z. Alvarez, A.N. Kolberg-Edelbrock, I.R. Sasselli, J.A. Ortega, R. Qiu, Z. Syrgiannis, P.A. Mirau, F. Chen, S.M. Chin, S. Weigand, E. Kiskinis, S.I. Stupp, Bioactive scaffolds with enhanced supramolecular motion promote recovery from spinal cord injury, Science 374 (6569) (2021) 848–856.

[42] Y. Shang, C. Ma, J. Zhang, Z. Wang, C. Ren, X. Luo, R. Peng, J. Liu, J. Mao, Y. Shi, G. Fan, Bifunctional supramolecular nanofiber inhibits atherosclerosis by enhancing plaque stability and anti-inflammation in apoE(-/-) mice, Theranostics 10 (22) (2020) 10231–10244.

[43] Z. Zhang, L. Li, W. Yang, Y. Cao, Y. Shi, X. Li, Q. Zhang, The effects of different doses of IGF-1 on cartilage and subchondral bone during the repair of full-thickness articular cartilage defects in rabbits, Osteoarthritis Cartilage 25 (2) (2017) 309–320.

[44] S. Lu, J. Lam, J.E. Trachtenberg, E.J. Lee, H. Seyednejad, J. van den Beucken, Y. Tabata, M.E. Wong, J.A. Jansen, A.G. Mikos, F.K. Kasper, Dual growth factor delivery from bilayered, biodegradable hydrogel composites for spatially-guided osteochondral tissue repair, Biomaterials 35 (31) (2014) 8829–8839.

[45] M.K. Boushell, C.Z. Mosher, G.K. Suri, S.B. Doty, E.J. Strauss, E.B. Hunziker, H. H. Lu, Polymeric mesh and insulin-like growth factor 1 delivery enhance cell homing and graft-cartilage integration, Ann. N. Y. Acad. Sci. 1442 (1) (2019) 138–152.

[46] J.W. Nichol, S.T. Koshy, H. Bae, C.M. Hwang, S. Yamanlar, A. Khademhosseini, Cell-laden microengineered gelatin methacrylate hydrogels, Biomaterials 31 (21) (2010) 5536–5544.

[47] E. Altan, K. Aydin, O. Erkocak, H. Senaran, S. Ugras, The effect of platelet-rich plasma on osteochondral defects treated with mosaicplasty, Int. Orthop. 38 (6) (2014) 1321–1328.

[48] B.B. Christensen, C.B. Foldager, M.L. Olesen, L. Vingtoft, J.H. Rolfing, S. Ringgaard, M. Lind, Experimental articular cartilage repair in the Gottingen minipig: the influence of multiple defects per knee, J. Exp. Orthop. 2 (1) (2015) 13.

[49] M.P. van den Borne, N.J. Raijmakers, J. Vanlauwe, J. Victor, S.N. de Jong, J. Bellemans, D.B. Saris, S. International, Cartilage repair, international cartilage repair society (ICRS) and oswestry macroscopic cartilage evaluation scores validated for use in autologous chondrocyte implantation (ACI) and microfracture, Osteoarthritis Cartilage 15 (12) (2007) 1397–1402.

[50] X. Guo, H. Park, S. Young, J.D. Kretlow, J.J. van den Beucken, L.S. Baggett, Y. Tabata, F.K. Kasper, A.G. Mikos, J.A. Jansen, Repair of osteochondral defects with biodegradable hydrogel composites encapsulating marrow mesenchymal stem cells in a rabbit model, Acta Biomater. 6 (1) (2010) 39–47.

[51] Y. Xu, G.K. Kong, J.G. Menting, M.B. Margetts, C.A. Delaine, L.M. Jenkin, V. V. Kiselyov, P. De Meyts, B.E. Forbes, M.C. Lawrence, How ligand binds to the type 1 insulin-like growth factor receptor, Nat. Commun. 9 (1) (2018) 821.

[52] A. Wu, Y. Guo, X. Li, H. Xue, J. Fei, J. Li, Co-assembled supramolecular gel of dipeptide and pyridine derivatives with controlled chirality, Angew Chem. Int. Ed. Engl. 60 (4) (2021) 2099–2103.

[53] X. Liu, J. Fei, A. Wang, W. Cui, P. Zhu, J. Li, Transformation of dipeptide-based organogels into chiral crystals by cryogenic treatment, Angew Chem. Int. Ed. Engl. 56 (10) (2017) 2660–2663.

[54] X. Ren, Q. Zou, C. Yuan, R. Chang, R. Xing, X. Yan, The dominant role of oxygen in modulating the chemical evolution pathways of tyrosine in peptides: dityrosine or melanin, Angew Chem. Int. Ed. Engl. 58 (18) (2019) 5872–5876.

[55] X. Meng, S. Grad, C. Wen, Y. Lai, M. Alini, L. Qin, X. Wang, An impaired healing model of osteochondral defect in papain-induced arthritis, J Orthop Translat 26 (2021) 101–110.

[56] E. Ruvinov, T. Tavor Re'em, F. Witte, S. Cohen, Articular cartilage regeneration using acellular bioactive affinity-binding alginate hydrogel: a 6-month study in a mini-pig model of osteochondral defects, J Orthop Translat 16 (2019) 40–52.

[57] L. Gao, M. Cucchiarini, H. Madry, Cyst formation in the subchondral bone following cartilage repair, Clin. Transl. Med. 10 (8) (2020) e248.
[58] M.L. Reilingh, C.J. van Bergen, L. Blankevoort, R.M. Gerards, I.C. van Eekeren, G. M. Kerkhoffs, C.N. van Dijk, Computed tomography analysis of osteochondral defects of the talus after arthroscopic debridement and microfracture, Knee Surg. Sports Traumatol. Arthrosc. 24 (4) (2016) 1286–1292.
[59] P. Orth, M. Cucchiarini, G. Kaul, M.F. Ong, S. Graber, D.M. Kohn, H. Madry, Temporal and spatial migration pattern of the subchondral bone plate in a rabbit osteochondral defect model, Osteoarthritis Cartilage 20 (10) (2012) 1161–1169.
[60] Z. Zamli, K. Robson Brown, J.F. Tarlton, M.A. Adams, G.E. Torlot, C. Cartwright, W.A. Cook, K. Vassilevskaja, M. Sharif, Subchondral bone plate thickening precedes chondrocyte apoptosis and cartilage degradation in spontaneous animal models of osteoarthritis, BioMed Res. Int. 2014 (2014), 606870.
[61] M.L. Reilingh, K.T.A. Lambers, J. Dahmen, K.T.M. Opdam, G. Kerkhoffs, The subchondral bone healing after fixation of an osteochondral talar defect is superior in comparison with microfracture, Knee Surg. Sports Traumatol. Arthrosc. 26 (7) (2018) 2177–2182.
[62] F. Zhou, Y. Hong, R. Liang, X. Zhang, Y. Liao, D. Jiang, J. Zhang, Z. Sheng, C. Xie, Z. Peng, X. Zhuang, V. Bunpetch, Y. Zou, W. Huang, Q. Zhang, E.V. Alakpa, S. Zhang, H. Ouyang, Rapid printing of bio-inspired 3D tissue constructs for skin regeneration, Biomaterials 258 (2020), 120287.
[63] K. Yue, G. Trujillo-de Santiago, M.M. Alvarez, A. Tamayol, N. Annabi, A. Khademhosseini, Synthesis, properties, and biomedical applications of gelatin methacryloyl (GelMA) hydrogels, Biomaterials 73 (2015) 254–271.
[64] R. Goto, E. Nishida, S. Kobayashi, M. Aino, T. Ohno, Y. Iwamura, T. Kikuchi, J. I. Hayashi, G. Yamamoto, M. Asakura, A. Mitani, Gelatin methacryloyl-riboflavin (GelMA-RF) hydrogels for bone regeneration, Int. J. Mol. Sci. 22 (4) (2021).
[65] L.S. Moreira Teixeira, J. Patterson, F.P. Luyten, Skeletal tissue regeneration: where can hydrogels play a role? Int. Orthop. 38 (9) (2014) 1861–1876.
[66] E. Arslan, I.C. Garip, G. Gulseren, A.B. Tekinay, M.O. Guler, Bioactive supramolecular peptide nanofibers for regenerative medicine, Adv. Healthc. Mater. 3 (9) (2014) 1357–1376.
[67] T. Burnouf, D. Strunk, M.B. Koh, K. Schallmoser, Human platelet lysate: replacing fetal bovine serum as a gold standard for human cell propagation? Biomaterials 76 (2016) 371–387.
[68] Y. Shang, M. Kuang, Z. Wang, Y. Huang, L. Liu, X. Zhao, R. Zhang, Y. Zhao, R. Peng, S. Sun, Q. Yang, Z. Yang, An ultrashort peptide-based supramolecular hydrogel mimicking IGF-1 to alleviate glucocorticoid-induced sarcopenia, ACS Appl. Mater. Interfaces 12 (31) (2020) 34678–34688.
[69] H. Wang, Y. Shang, X. Chen, Z. Wang, D. Zhu, Y. Liu, C. Zhang, P. Chen, J. Wu, L. Wu, D. Kong, Z. Yang, Z. Li, X. Chen, Delivery of MSCs with a hybrid beta-sheet peptide hydrogel consisting IGF-1C domain and D-form peptide for acute kidney injury therapy, Int. J. Nanomed. 15 (2020) 4311–4324.
[70] L. Yan, G. Liu, X. Wu, Exosomes derived from umbilical cord mesenchymal stem cells in mechanical environment show improved osteochondral activity via upregulation of LncRNA H19, J Orthop Translat 26 (2021) 111–120.
[71] R. Motalleb, E.J. Berns, P. Patel, J. Gold, S.I. Stupp, H.G. Kuhn, In vivo migration of endogenous brain progenitor cells guided by an injectable peptide amphiphile biomaterial, J. Tissue Eng. Regen. Med. 12 (4) (2018) e2123–e2133.
[72] E.J. Berns, S. Sur, L. Pan, J.E. Goldberger, S. Suresh, S. Zhang, J.A. Kessler, S. I. Stupp, Aligned neurite outgrowth and directed cell migration in self-assembled monodomain gels, Biomaterials 35 (1) (2014) 185–195.
[73] D. Lin, Y. Chai, Y. Ma, B. Duan, Y. Yuan, C. Liu, Rapid initiation of guided bone regeneration driven by spatiotemporal delivery of IL-8 and BMP-2 from hierarchical MBG-based scaffold, Biomaterials 196 (2019) 122–137.
[74] M.S. Park, Y.H. Kim, Y. Jung, S.H. Kim, J.C. Park, D.S. Yoon, S.H. Kim, J.W. Lee, In situ recruitment of human bone marrow-derived mesenchymal stem cells using chemokines for articular cartilage regeneration, Cell Transplant. 24 (6) (2015) 1067–1083.
[75] Y.S. Liu, M.E. Ou, H. Liu, M. Gu, L.W. Lv, C. Fan, T. Chen, X.H. Zhao, C.Y. Jin, X. Zhang, Y. Ding, Y.S. Zhou, The effect of simvastatin on chemotactic capability of SDF-1alpha and the promotion of bone regeneration, Biomaterials 35 (15) (2014) 4489–4498.
[76] J. Ratanavaraporn, H. Furuya, H. Kohara, Y. Tabata, Synergistic effects of the dual release of stromal cell-derived factor-1 and bone morphogenetic protein-2 from hydrogels on bone regeneration, Biomaterials 32 (11) (2011) 2797–2811.
[77] X. Shen, Y. Zhang, Y. Gu, Y. Xu, Y. Liu, B. Li, L. Chen, Sequential and sustained release of SDF-1 and BMP-2 from silk fibroin-nanohydroxyapatite scaffold for the enhancement of bone regeneration, Biomaterials 106 (2016) 205–216.
[78] S. Illien-Junger, G. Pattappa, M. Peroglio, L.M. Benneker, M.J. Stoddart, D. Sakai, J. Mochida, S. Grad, M. Alini, Homing of mesenchymal stem cells in induced degenerative intervertebral discs in a whole organ culture system, Spine 37 (22) (2012) 1865–1873 (Phila Pa 1976).
[79] G.A. Rico-Llanos, J. Becerra, R. Visser, Insulin-like growth factor-1 (IGF-1) enhances the osteogenic activity of bone morphogenetic protein-6 (BMP-6) in vitro and in vivo, and together have a stronger osteogenic effect than when IGF-1 is combined with BMP-2, J. Biomed. Mater. Res. 105 (7) (2017) 1867–1875.
[80] S. Kim, Y. Kang, C.A. Krueger, M. Sen, J.B. Holcomb, D. Chen, J.C. Wenke, Y. Yang, Sequential delivery of BMP-2 and IGF-1 using a chitosan gel with gelatin microspheres enhances early osteoblastic differentiation, Acta Biomater. 8 (5) (2012) 1768–1777.
[81] L. Zhou, V.O. Gjvm, J. Malda, M.J. Stoddart, Y. Lai, R.G. Richards, K. Ki-Wai Ho, L. Qin, Innovative tissue-engineered strategies for osteochondral defect repair and regeneration: current progress and challenges, Adv. Healthc. Mater. (2020), e2001008.
[82] K.M. Yamada, M. Sixt, Mechanisms of 3D cell migration, Nat. Rev. Mol. Cell Biol. 20 (12) (2019) 738–752.
[83] C. Gaggioli, S. Hooper, C. Hidalgo-Carcedo, R. Grosse, J.F. Marshall, K. Harrington, E. Sahai, Fibroblast-led collective invasion of carcinoma cells with differing roles for RhoGTPases in leading and following cells, Nat. Cell Biol. 9 (12) (2007) 1392–1400.
[84] S. Wong, W.H. Guo, Y.L. Wang, Fibroblasts probe substrate rigidity with filopodia extensions before occupying an area, Proc. Natl. Acad. Sci. U. S. A. 111 (48) (2014) 17176–17181.